ADVANCED FUNCTIONAL MATERIALS
www.afm-journal.de

Continuous-Flow Photocatalytic Degradation of Glyphosate and Aminomethylphosphonic Acid Under Simulated Sunlight with TiO_2-Coated Poly(vinylidene fluoride) Membrane

*Phuong B. Trinh, Siqi Liu, Nurul F. Himma, Béla Fiser, and Andrea I. Schäfer**

Degradation of glyphosate (GLY) and its primary metabolite, aminomethylphosphonic acid (AMPA) is investigated at environmentally relevant concentrations using a poly(vinylidene fluoride) membrane with immobilized titanium dioxide (PVDF-TiO_2) in a continuous flow-through operation. The photocatalytic degradation under the solar spectrum (AM1.5 g 350–1150 nm) is comparable with that under UV Light (365 nm) at equivalent absorbed irradiance with 63–65% GLY and 21–25% AMPA removal. Hence, non-UV wavelengths do not contribute to degradation. The limiting factors affecting degradation (irradiance, flux, initial concentration, and pH) are investigated. The scavenger study indicated $\bullet O_2^-$ as the primary contributor to GLY/AMPA degradation, while h_{VB}^+ played a significant role as well. One of the most possible degradation pathways for GLY and AMPA in the photocatalytic membrane reactor is elucidated using the G3MP2B3 composite method via bond dissociation enthalpy (BDE) values. GLY degradation to AMPA and oxalic acid is identified as the preferred pathway due to the weak C—N bond. Under optimized conditions (highest irradiance of 98 mW cm^{-2}, and lowest flux of 60 L m^{-2} h^{-1}), 95% GLY and 80% AMPA are removed by the PVDF-TiO_2 membrane. The potential of photocatalytic membranes for the degradation of low molecular-weight, charged micropollutants in continuous operations is highlighted.

1. Introduction

1.1. GLY and AMPA in the Water Environment

Glyphosate (N-(phosphonomethyl) glycine, GLY) was introduced in the 1970s under the trade name Roundup by Monsanto, USA, and has since become the most widely used herbicide globally.[1,2] Aminomethylphosphonic acid (AMPA), the primary metabolite of GLY, is formed via C—N bond cleavage[3] and is frequently detected in surface waters alongside GLY.[4,5] AMPA exhibits similar toxicity to GLY and is more thermodynamically stable.[6,7] Exposure to GLY has been linked to DNA damage, cytotoxic effects, reduced male fertility, cancer, and endocrine disruption.[8–11] Due to these severe health effects, more than 177000 lawsuits have been filed against Roundup, resulting in Monsanto (now Bayer) paying nearly $16 billion for settlements.[12] Schwientek et al. claimed that aminopolyphosphonates in laundry detergents were the main source of GLY in European rivers, rather than agricultural runoff, as was previously thought.[13] This finding added up to the debate on whether GLY should be banned in Europe.[14] Despite environmental and public health concerns, the European Commission renewed the marketing authorization for GLY until 2033, allowing its continued use in agriculture (covering 30% of the acreage for annual crops and 50% for perennial tree crops).[15–17] With the expanding usage of GLY, the increasing concentration of GLY and AMPA can reach surface and groundwaters via leaching.[18] GLY and AMPA have been detected in European surface waters at concentrations of up to 370

P. B. Trinh, S. Liu, N. F. Himma, A. I. Schäfer
Institute for Advanced Membrane Technology (IAMT)
Karlsruhe Institute of Technology (KIT)
Hermann-von-Helmholtz-Platz 1, 76344 Eggenstein-Leopoldshafen, Germany
E-mail: Andrea.Iris.Schaefer@kit.edu

The ORCID identification number(s) for the author(s) of this article can be found under https://doi.org/10.1002/adfm.202511431

DOI: 10.1002/adfm.202511431

B. Fiser
Department of Physical Chemistry
Faculty of Chemistry
University of Lodz
Pomorska 163/165, Łódź 90-236, Poland

B. Fiser
Institute of Chemistry, Faculty Materials and Chemical Engineering
University of Miskolc
Miskolc-Egyetemváros 3515, Hungary

and 200 µg L^{-1}, respectively,[19–21] while in Germany, GLY and AMPA concentration at 1 µg L^{-1} was reported in surface water.[22] Such concentrations in water supplies require advanced treatment technologies to meet the European Union (EU) drinking water guidelines of 100 ng L^{-1} for each herbicide and 500 ng L^{-1} for total herbicide concentration.[23]

1.2. Limitations of Current GLY and AMPA Removal Technologies

Due to the small molecular weight of GLY (169 g mol^{-1}) and AMPA (111 g mol^{-1}) and their complex physiochemical properties (strongly polar, hydrophilic, and non-volatile), conventional water treatment technologies could not remove GLY and AMPA effectively.[24,25] Coagulation and flocculation achieve poor removal of <20%[26]; while electrocoagulation was reported to increase removal to 30–40%.[27] Various adsorbents, including activated carbon,[28,29] biochar,[30,31] multi-walled carbon nanotubes,[32] resins,[33] metal–organic frameworks (MOFs),[34,35] magnetite nanoparticles[36] could effectively remove 50–90% GLY and AMPA. Even for commercial materials, the regeneration remains a challenge.[37] Membrane technologies such as nanofiltration (NF) and reverse osmosis (RO) are semi-permeable barriers that partially remove 70–90% GLY.[38–41] However, these processes require high energy inputs (pressures up to 25 bar),[39] pre-treatment,[42,43] and require further concentrate treatment to eliminate micropollutants.[44]

Advanced oxidation processes (AOPs) have emerged as promising alternatives with rapid degradation and non-selective oxidation.[45] Ozonation and ultrasonication could remove 45–80% GLY from water at an initial concentration > 30 mg L^{-1}.[46,47] Photo-Fenton[48–50] and electro-Fenton[51,52] have been applied for GLY degradation in the presence of iron, with the removal of 40–80% from the initial concentration of 5–10 mg L^{-1}. Tran et al. used Ti/PbO_2 anode for GLY electrochemical degradation, which could remove > 90% from an initial concentration of 16.9 mg L^{-1}.[53] However, some AOPs techniques can produce hazardous by-products, such as ozonation forming non-biodegradable bromates.[54] Furthermore, the stability of reactive oxygen species (ROS) precursors can also limit the performance of AOPs in micropollutant degradation.[55,56] Among different AOPs, heterogeneous photocatalysis using light-activated semiconductors provides advantages for degrading persistent micropollutants, including high degradation efficiency, cost-effectiveness, elimination of chemical additives, and reusable catalyst systems,[57] even though up-scale to pilot operations has not been implemented.

1.3. TiO_2 Photocatalytic Degradation of GLY and AMPA

Titanium dioxide (TiO_2) has been extensively researched for photocatalytic degradation due to its physical and chemical stability, low cost, and exceptional photocatalytic activity.[58–60] Owing to the potential oxidizing capacity of generated ROS, TiO_2-mediated photocatalysis effectively degrades GLY, along with its primary degradation intermediate AMPA.[46] Commercial Aeroxide© TiO_2–P25 has been investigated for GLY degradation in batch experiments, with the removal of > 90% from an initial concentration of 25 mg L^{-1}.[61] TiO_2 has also been coated onto various materials, such as magnetic $NiFe_2O_4$,[62] graphene,[63] enhancing GLY removal from 65% to > 90%. However, most studies on GLY photocatalytic degradation have used high feed concentrations (in mg/L),[63,64] owing probably to analytical challenges. However, environmentally relevant concentrations in the nano- or microgram-per-litre range,[65,66] tend to exhibit different reaction kinetics and transport behaviors due to the typical mass transfer limitations of micropollutants.[67]

TiO_2 photocatalytic efficiency is limited by the rapid charge recombination of electron-hole pairs and its wide bandgap (3.0–3.2 eV[68,69]), which restricts activity under visible light.[70,71] As a result, most TiO_2-based photocatalysis studies on GLY degradation have been conducted under UVA irradiation,[72–74] which has the maximum absorption wavelength (λ_{max}) ≈400 nm.[75] However, the need to reduce carbon emissions from fossil fuel-based electricity generation has driven the research under UV light to photocatalysis powered by solar energy.[76,77] Although only 5% of solar radiation reaching the Earth's surface lies in the UV spectrum,[78,79] TiO_2 photocatalysis remains viable under solar irradiation, even though much less efficient, and has been shown to effectively degrade pollutants in water.[80,81] Amiri and Anbia have used a carbon-doped TiO_2/clinoptilolite nanocomposite for GLY degradation under visible light, which can remove 84% GLY from an initial concentration of 30 mg L^{-1}, and AMPA was found in the degradation products in batch experiments.[82] Therefore, GLY and AMPA degradation by TiO_2 under solar light at environmentally relevant conditions remains an area of interest.

1.4. Photocatalytic Membrane Reactors

Photocatalytic membrane reactors consist of either a suspended catalyst in suspension prior to a membrane or one that is immobilized in a membrane. Suspension-based photocatalysis technologies face several challenges, including reduced light penetration due to photocatalyst agglomeration, turbidity effects, catalyst recovery, and mass transport of reactants and ROS.[83,84] Chen et al. determined that TiO_2 loading was a limiting factor for GLY degradation in batch, where more ROS was produced; however, further increase in TiO_2 loading could prevent light penetration and might cause catalyst agglomeration.[72,73] Photocatalytic membrane reactors (PMRs) integrate photocatalysis with membrane filtration in a single unit, typically by immobilizing the catalyst into a membrane. This overcomes the need for photocatalyst recovery and reduces catalyst agglomeration of suspended systems.[85–87] For micropollutant degradation, mass transfer is the main limitation of both batch and photocatalytic membrane reactors.[87] This can be mitigated in a turbulent flow operation[88] and through diffusion-driven transport at low membrane fluxes, while in small membrane pores, boundary layer phenomena are minimized. Membrane photocatalysis offers a high surface-to-volume ratio, improves contact between pollutants and catalysts, which overcomes common drawbacks of batch systems.[89,90] TiO_2 has been successfully integrated into membranes to enhance the removal of micropollutants, such as steroid hormones[91] and pharmaceuticals,[92,93] with reported removal > 90%. TiO_2-based photocatalytic membranes for GLY and

AMPA degradation from water have not yet been reported, even though mechanisms appear feasible.

1.5. Mechanisms of GLY and AMPA Photocatalysis Degradation by TiO_2

Photocatalysis involves the absorption of photons by TiO_2, which leads to the excitation of electrons from the valence band to the conduction band (e^-_{CB}) and generates electron holes in the valence band (h^+_{VB}).[94,95] These charge carriers can directly degrade pollutants adsorbed on the TiO_2 surface. Additionally, the photoinduced charge species participate in redox reactions with oxygen and water, resulting in the sequential production of ROS, which degrade various persistent micropollutants.[96] h^+_{VB} can oxidize water molecules (H_2O) or hydroxide ions (OH^-) to create hydroxyl radicals (•OH), which are the primary species formed and the dominant ROS. With a redox potential of $E^{\theta}_{\bullet OH/H_2O}$ = +2.8 V,[97,98] •OH facilitates the non-selective oxidation of diverse organic pollutants. Meanwhile, e^-_{CB} can reduce oxygen molecules to form superoxide radicals ($\bullet O_2^-$) which despite having a lower reactivity than •OH, can be produced by oxygen reduction with a redox potential of $E^{\theta}_{O_2^{\bullet-}/H_2O_2,H^+}$ = +0.94 V.[99] The photodetachment of electrons from $\bullet O_2^-$ results in the formation of singlet oxygen ($^1O_2$, $E^{\theta}_{^1O_2/O_2^-}$ = +0.65 V[100]), which is the primary mechanism for its formation in TiO_2 photocatalysis.[101]

GLY and AMPA degradation involves the oxidation by ROS, which can occur through two main pathways: i) C—N bond cleavage to produce AMPA and glyoxylic acid, and ii) C—P bond cleavage to produce sarcosine, which is then degraded to glycine.[102] The latter pathway is preferred due to the formation of safer intermediate products.[64,102,103] However, the C—P bond in phosphonic acids is thermally stable and chemically resistant, which is associated with its high bond energy.[104] The reaction rates of GLY and AMPA with ROS follow the first-order kinetics ($A + B \rightarrow C$), depending on the concentrations of GLY/AMPA and the rate constant ($r = \mathrm{k} \cdot [ROS][GLY]$)

$$(r = k \cdot [ROS] \cdot [GLY]) \quad (1)$$

The degradation mechanisms of GLY and AMPA become more complex in synthetic and real water matrices due to the presence of ROS scavengers (e.g., CO_3^{2-}, HCO_3^-), which compete with GLY and AMPA for ROS reactions, thereby leading to incomplete degradation.[105,106] While the identification of metabolites is extremely challenging, in particular in relevant concentrations, computational chemistry allows to identify of most likely pathways.

1.6. Computational Chemistry Calculations of GLY and AMPA

Analysis of likely electron transfer pathways in micropollutant molecules and free radical attack mechanisms is critical to address environmental persistence and potential formation of hazardous by-products.[61] Understanding the fate of GLY and AMPA in degradation is environmentally essential, as incomplete transformation may result in the release of stable, harmful residues into aquatic ecosystems, posing risks to biodiversity and human health.[10] In complex photocatalysis systems, the coexistence of multiple ROS may lead to different degradation pathways, some of which could produce more toxic intermediates than the parent compounds (i.e., methylphosphonic acid or nitrosamines).[61,107] Quantum chemical calculations has proven to be a powerful tool to obtain deeper insight into reaction mechanisms, as well as offer a very valuable complement to experimental studies.[108,109] Sadatsharifi et al. used density functional theory (DFT) to investigate the possible breakdown pathway of GLY by photodegradation in different environments, which was influenced by the type of radical species and pH.[110] The photodegradation of GLY by manganese oxide and UV light showed that the favour degradation pathway depended on the ratio of photocatalyst and GLY.[111] The degradation of GLY and AMPA was influenced by the solvents, where solvent interactions affected stability.[112] Limitations of previous research lie in the detailed knowledge about the reaction pathways, especially for the evolution of intermediates, because of the difficulties in experimental investigation of the complex intermediate structure.

There are several computational chemistry tools available, including various density functional theory and ab initio methods, but to get accurate thermochemical properties, proper method selection is inevitable by considering the features of the studied system.[113] As the degradation process of the molecules, GLY and AMPA, considered in this project includes the formation of radical species, bond dissociation enthalpies have to be determined to describe fragmentation pathways. Therefore, the selected method has to be able to handle radical species and provide accurate thermochemical properties. One of the most suitable computational tools is the G3MP2B3 composite quantum chemistry method, which has been proven to be applicable for such systems numerous times.[114,115] G3MP2B3 belongs to the family of Gaussian-3 (G3) theory methods. It was developed to be efficient in terms of computational cost without compromising accuracy.[116,117] The G3MP2B3 protocol includes geometry optimisations and frequency calculations at the B3LYP/6-31G(d) level of theory (B3).[116,117] Additional single-point energy calculations are also carried out on the optimized structures within the G3MP2B3 protocol, to finetune the accuracy of the determined energies. These include QCISD (Quadratic Configuration Interaction with Singles and Doubles) and MP2 (second order Møller-Plesset perturbation theory) calculations.[116,117] All in all, the DFT-based geometry (B3) and the additional single-point calculations (QCISD and MP2) with the proper protocol in place provide an accurate and reliable computational tool to determine the thermochemical properties.

This research investigates the removal of GLY and AMPA in water at the environmentally relevant concentration using a photocatalytic membrane in a flow-through configuration. The degradation performance of a PVDF-TiO_2 membrane under simulated sunlight is compared to that under UV light, with an evaluation of limiting factors in GLY/AMPA photocatalytic degradation. Additionally, the interplay between ROS dynamics and matrix effects is explored to determine the degradation pathways of GLY and AMPA by determining the corresponding bond dissociation enthalpy values using the G3MP2B3 composite method, which uses the Gaussian-3 theory (G3) as a high-level ab initio method to calculate molecular energies, where the Møller-Plesset perturbation theory (MP) is a method used to improve the

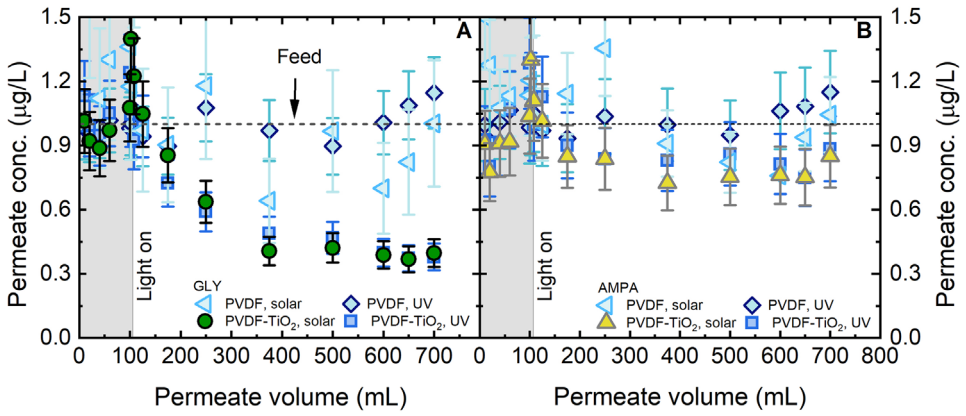

Figure 1. GLY (A) and AMPA (B) permeate concentration versus cumulated permeate volume under solar simulator and UV light (PVDF and PVDF-TiO_2, c_f (GLY/AMPA) = 1 µg L^{-1}, J_w= 600 L m^{-2} h^{-1}, I (AM1.5 g 350–1150 nm) = 50 mW cm^{-2}, I (365 nm) = 2.1 mW cm^{-2}, pH 8.1 ± 0.2, 23 ± 1 °C).

accuracy of ab initio calculations and the geometries and zero-point vibrational energies are calculated using the B3LYP density functional theory (DFT).

2. Results and Discussion

To evaluate the photocatalytic degradation performance, the removal of GLY and AMPA was examined under both UV and solar light. The limiting factors affecting photodegradation were then systematically investigated. The photodegradation pathway was analyzed using the G3MP2B3 composite computational chemistry method, which was employed to determine all unique BDE values. Finally, an optimized experiment was conducted where limiting factors were reduced to determine whether GLY and AMPA removal is able to meet EU regulatory requirements in principle. The standard experimental conditions are shown in Table S1 (Supporting Information), and the operating parameters are presented in Figures S1–S12 (Supporting Information).

2.1. Photocatalytic Degradation with Simulated Solar Light and UV Light

The removal efficiency of GLY and AMPA through photolysis and photocatalysis was assessed by comparing degradation performance under simulated solar light (350—1150 nm, 50 mW cm^{-2}) and UV light (365 nm, 2.1 mW cm^{-2}) to determine the feasibility of using solar irradiation for effective removal (**Figure 1**). The irradiance was adjusted to reflect the UV light in the simulated solar light. By integrating the solar irradiance in the wavelength < 400 nm, UV irradiance accounts for 4.2% of the simulated solar irradiance (Figure S13, Supporting Information). Hence, the solar irradiance at 50 mW cm^{-2} is equivalent to UV irradiance at 2.1 mW cm^{-2}. GLY and AMPA were prepared in a mixture as GLY and AMPA typically coexist in the environment at a concentration of 1 µg L^{-1} each, as observed in Germany.[22]

In the absence of TiO_2, no significant degradation of GLY or AMPA was observed when comparing UV and simulated solar light at the chosen irradiance values (Figure 1). The permeate concentrations of GLY and AMPA were 0.9–1 ± 0.1 µg L^{-1} when the pristine membrane was used for filtration (Figure 1), indicating that no measurable photolysis took place. Papagiannaki et al. reported that GLY photolysis occurred under UV light (wavelength 254 nm, irradiance ≈23 J cm^{-2}) in batch experiments and achieved 90% degradation in water.[118] However, in this study, photolysis was not observed in dynamic filtration, possibly due to the high flux or low hydraulic residence time (Figure S14, Supporting Information), which reduced the contact time between GLY/AMPA, and UV light. A similar phenomenon was observed in a dark-phase experiment, where the permeate concentrations were 1 ± 0.1 µg L^{-1}, indicating no adsorption of GLY or AMPA onto the PVDF-TiO_2 membrane (Figure S15, Supporting Information). Since photolysis and membrane adsorption did not contribute to GLY and AMPA removal, photocatalytic degradation by the PVDF-TiO_2 membrane can be investigated.

GLY and AMPA degradation was observed under both UV and simulated solar light with the PVDF-TiO_2 membrane. Under UV light ($I_{365\,nm}$ = 2.1 mW cm^{-2}), the permeate concentration decreased from 1 ± 0.1 µg L^{-1} (feed solution) to 0.4 ± 0.06 µg L^{-1} for GLY and 0.8 ± 0.1 µg L^{-1} for AMPA (Figure 1). This photodegradation was anticipated, as TiO_2-based photocatalysis for GLY degradation is well-established under UV irradiation.[72–74] Under simulated solar light, the permeate concentration decreased from 1 ± 0.1 µg L^{-1} to 0.4 ± 0.06 µg L^{-1} for GLY and 0.8 ± 0.1 µg L^{-1} for AMPA (Figure 1), this comparable reduction observed under simulated solar light suggests that non-UV solar spectra does not contribute to degradation. This conclusion was further supported by filtration experiments conducted at different wavelengths (Figure S16, Supporting Information).

Removal and rate of disappearance (r_i'') for GLY and AMPA under 350–1150 nm were comparable to those observed under 365 nm. Specifically, GLY removal was 65 ± 6% under 350—1150 nm and 63 ± 6% under 365 nm, while AMPA removal was 25 ± 6% and 20 ± 7 %, respectively. The corresponding r_i'' values were (6–7) ± 1 · 10^{10} mol m^{-2} $^{-1}s^{-1}$ for GLY and 3 ± 0.5 · 10^{10} mol m^{-2} $^{-1}s^{-1}$ for AMPA. Meanwhile, at wavelengths of 400–1150 nm (non-UV range), both removal and r_i'' values were negligible, confirming that non-UV wavelengths did not contribute to GLY and AMPA degradation.

Under both UV and solar light, the permeate concentration of GLY was consistently lower than that of AMPA, with values of 0.4

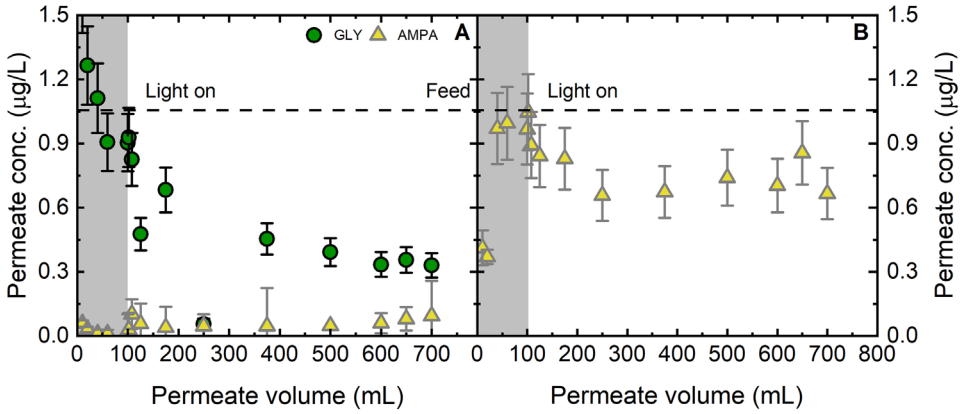

Figure 2. Permeate concentration (c_p) versus cumulated permeate volume with individual GLY (A) and individual AMPA (B) (PVDF-TiO_2, c_f (GLY/AMPA) = 1 µg L^{-1}, J_w = 600 L m^{-2} h^{-1}, I (AM1.5 g 350–1150 nm) = 50 mW cm^{-2}, pH 8.1 ± 0.2, and 23 ± 1 °C).

± 0.06 µg L^{-1} for GLY and 0.8 ± 0.1 µg L^{-1} for AMPA (Figure 1). The photodegradation of AMPA was insignificant, which was also found in previous research on AMPA degradation.[48,119] Furthermore, the r_i'' value for GLY (6 ± 1 · 10^{10} mol m^{-2} s^{-1}) was about twice that of AMPA (3 ± 0.5 · 10^{10} mol m^{-2} $^{-1}s^{-1}$) (Figure S16, Supporting Information). The higher degradation rates for GLY and AMPA could be attributed to either i) the greater stability of AMPA compared to GLY,[120] or ii) AMPA generation as an intermediate product during GLY degradation, which will be examined in subsequent sections.

2.2. Individual GLY and AMPA Degradation

To investigate whether AMPA forms as a degradation product of GLY degradation, the photocatalytic degradation of GLY and AMPA was examined individually under simulated solar light (AM1.5G, 350–1150 nm, irradiance = 50 mW cm^{-2}) (**Figure 2**).

During individual photodegradation experiments, the permeate concentration of GLY remained lower than that of AMPA, indicating a higher degradation for GLY than AMPA by the PVDF-TiO_2 membrane under solar light (Figure 2). AMPA did not show a significant increase in concentration during the experiment. In fact, AMPA is known to be more persistent than GLY,[121] which results a lower and slower degradation compared to GLY (as can also be seen in Figure 1; Figure S16, Supporting Information). Furthermore, the degradation of GLY and AMPA by the TiO_2 catalyst has been reported to be influenced by adsorption onto the TiO_2 surface.[122] While adsorption was not measurable in the light phase, GLY and AMPA, as well as their photodegradation products, may adsorb onto TiO_2 and the membrane surface via hydrogen bonding, van der Waals interactions, and surface complexation with the phosphonate, amine, and carboxylate functional groups.[122,123] GLY has been reported to have a higher affinity for TiO_2 than AMPA due to the stronger functional group interactions[123] and higher molecular weight.[124] It is also possible that the degradation rate of GLY and AMPA is different, which means both the adsorption and degradation interplay, leading to higher apparent removal of GLY.

In the individual photodegradation of GLY (Figure 2A), there was no significant difference in GLY permeate concentration between the mixture (0.4 ± 0.1 µg L^{-1}, Figure 1A) and the individual experiment (0.3 ± 0.1 µg L^{-1}, Figure 2A), indicating that the presence of AMPA did not affect GLY degradation. In the individual photodegradation of AMPA, the permeate concentration (0.7 ± 0.1 µg L^{-1}, Figure 2B) was insignificantly lower than in the mixture (0.8 ± 0.1 µg L^{-1}, Figure 1B). A contribution of competition between GLY and AMPA for degradation sites,[125] or the formation of AMPA during GLY degradation[126] could thus not be determined. In Figure 2A, AMPA was detected in the permeate at a concentration of 0.1 ± 0.02 µg L^{-1} during GLY degradation, indicating a marginally higher permeate concentration of AMPA in the mixture than in the individual photodegradation experiment. The formation of AMPA in GLY photodegradation by TiO_2 has been reported in batch experiments, where AMPA was identified as a reaction intermediate.[61] The degradation of the GLY to AMPA pathway is indeed kinetically preferred,[110] increasing the possibility of AMPA formation even though no clear evidence is identifiable in these low hydraulic residence time experiments.

To gain deeper insight into the mechanism of GLY and AMPA degradation by the PVDF-TiO_2 membrane under simulated solar light, the rate-limiting steps were investigated under varying operating conditions, including irradiance, flux, and water quality (initial herbicide concentration and pH).

2.3. Photocatalytic Degradation of GLY/AMPA Enhancement by Irradiance

Light intensity determines the number of photons available for the photocatalyst surface, which would affect the reactive oxygen species (ROS) generation. To evaluate photon availability as a limiting factor for GLY and AMPA degradation, photocatalytic experiments were conducted under varying irradiance intensity for UV (0.4–4.1 mW cm^{-2}) and simulated solar light (10–98 mW cm^{-2}) (**Figure 3**).

Under UV light, GLY removal increased from 48 ± 6 to 68 ± 8% as UV irradiance increased from 0.4 to 4.1 mW cm^{-2} (Figure 3A), for AMPA, removal increased marginally from 10 ± 3 to 26 ± 7%, with significant error. The rate of disappearance (r_i'') increased from 5 ± 1 to 7 ± 1 · 10^{10} mol m^{-2} s^{-1} for GLY and from 1 ± 1

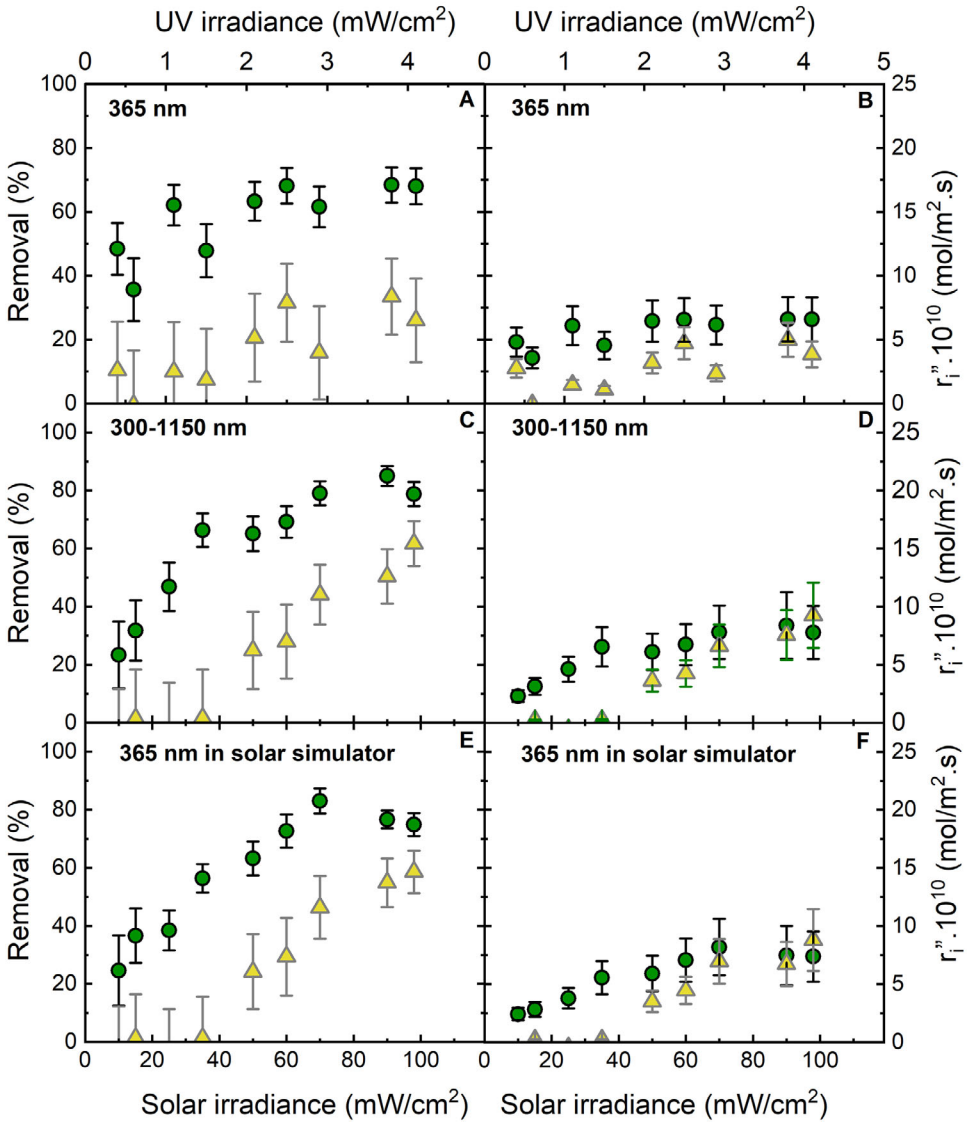

Figure 3. Removal and rate of disappearance (r_i'') of GLY and AMPA at varied irradiance of UV light (A, B), solar simulator (C, D), and UV channel in the solar simulator (E, F) (PVDF-TiO_2, c_f (GLY/AMPA) = 1 µg L^{-1}, J_w = 600 L m^{-2} h^{-1}, pH 8.1 ± 0.2, and 23 ± 1 °C). Intensity of light in the UV wavelengths induced by the solar irradiator (C and D) is equivalent to the intensity of UV light induced by the LED (A and B). Dotted lines are guides for the eye.

to 4 ± 1 · 10^{10} mol m^{-2} s^{-1} for AMPA (Figure 3B). The slight increase in GLY and AMPA degradation contradicts previous work on steroid hormone degradation by the same PVDF-TiO_2 membrane, where steroid hormone removal increased significantly from 10 to 74 ± 7% when increasing the UV irradiance from 0.5 to 5 mW cm^{-2}.[127] However, it is noted that the error bars between different irradiance of UV overlap, which hindered the effect of varying irradiance on the photodegradation of GLY and AMPA.

Under solar light, GLY removal increased significantly from 23 ± 6% to 79 ± 4% as solar irradiance increased from 10 to 70 mW cm^{-2}, then plateaued at 79–85% for irradiance > 70 mW cm^{-2} (Figure 3C). The r_i'' of GLY increased from 2 ± 0.3 · 10^{10} mol m^{-2} s^{-1} to 8 ± 2 · 10^{10} mol m^{-2} s^{-1} for the irradiance range from 10 to 70 mW cm^{-2}, stabilizing at 8 ± 2 · 10^{10} mol m^{-2} s^{-1} for irradiance > 70 mW cm^{-2} (Figure 3D). The significant increase in r_i'' at lower irradiance indicates an increase of electron-hole formation rate, which consequently increases the ROS production and enhances the removal of GLY under solar light.[128] Therefore, ROS generation is limited by photon availability. However, at higher irradiance (>70 mW cm^{-2}), r_i'' was stable at 8 ± 2 · 10^{10} mol m^{-2} s^{-1} which was attributed to electron-hole recombination, which makes r_i'' independent of light irradiance.[128]

Meanwhile, AMPA degradation commenced later, at an irradiance of 35 mW cm^{-2}, with removal increasing from 25 ± 6% to 62 ± 8% as irradiance rose from 50 to 98 mW cm^{-2} (Figure 3C). Below 35 mW cm^{-2}, no degradation was observed, with r_i'' of AMPA remaining < 10^{10} mol m^{-2} s^{-1}. This indicates that i) photon flux was insufficient to generate enough ROS for effective

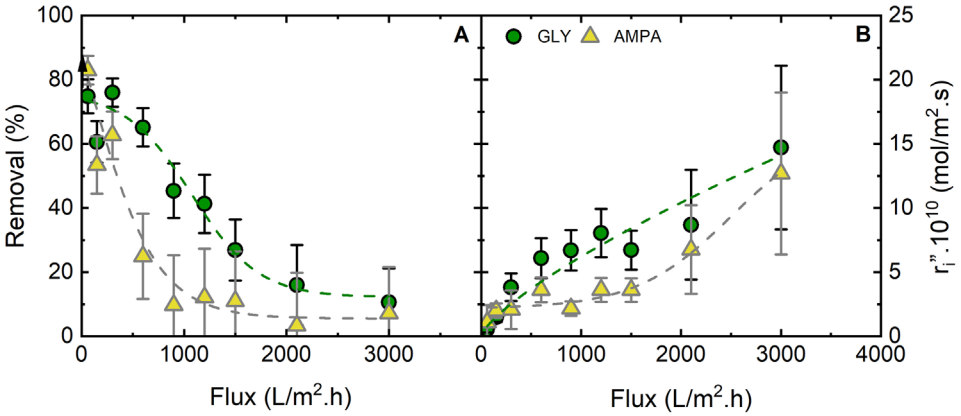

Figure 4. Removal (A) and rate of disappearance (r_i'') (B) of GLY/AMPA under solar simulator at varied water flux (PVDF-TiO_2, c_f (GLY/AMPA) = 1 µg L^{-1}, I (AM1.5 g 350–1150 nm) = 50 mW cm^{-2}, pH 8.1 ± 0.2, and 23 ± 1 °C). Dotted lines are guides for the eye.

AMPA degradation; ii) AMPA was less photodegradable than GLY. These findings reinforce the previous statement following Figure 2 that GLY is more degradable than AMPA. The slight difference in the removal and rate of disappearance of GLY and AMPA between UV and solar was contributed by the difference in light characteristics between the UV lamp and solar simulator (Figure 3E,F).

Since mass transfer is likely to be a limiting factor in the photodegradation of GLY and AMPA by the PVDF-TiO_2 membrane, due to the low herbicide concentrations, flux and initial concentration were further investigated.

2.4. Mass Transfer and Hydraulic Residence Time

Water flux determines the hydraulic residence time of micropollutants in contact with ROS and influences the molar flux of GLY and AMPA. To identify the threshold for a contact-time-independent region in GLY/AMPA removal, filtration experiments were conducted across a flux range of 60–3000 L m^{-2} h^{-1} (**Figure 4**). This flux range corresponds to a hydraulic residence time decrease from 4.5 to 0.09 s and a molar flux increase (that indicates the amount of herbicide brought to the membrane) from 10^{10} to 49 · 10^{10} mol m^{-2} s^{-1} for GLY and 10^{10} to 75 · 10^{10} mol m^{-2} s^{-1} for AMPA (Figure S14, Supporting Information).

Both GLY and AMPA removal decreased as flux increased from 60 to 1500 L m^{-2} h^{-1}, then stabilized at a flux > 2000 L m^{-2} h^{-1} (Figure 4A), which was associated with a reduction in hydraulic residence time from 4.5 to 0.09 s. GLY removal decreased from 75 ± 5% to 10 ± 9% as flux increased from 60 to 1500 L m^{-2} h^{-1} (with hydraulic residence time decreased from 4.5 to 0.2 s). At flux < 2000 L m^{-2} h^{-1}, GLY r_i'' increased from 10^{10} to 10 ± 3 · 10^{10} mol m^{-2} s^{-1}, corresponding to an increase in molar flux from 10^{10} to 25 · 10^{10} mol m^{-2} s^{-1} for GLY (Figure S14, Supporting Information). In essence, at a higher flux, less time is available to degrade more herbicide, which results in a concurrent reduction in removal and an increase in the rate of disappearance.

Similarly, AMPA removal decreased from 82 ± 4% to 7 ± 6% as flux increased from 60 to 1500 L m^{-2} h^{-1} (with hydraulic residence time decreasing from 4.5 to 0.2 s). AMPA r_i'' increased from 10^{10} to 4 ± 1 · 10^{10} mol m^{-2} s^{-1} at flux < 1500 L m^{-2} h^{-1}, associated with a rise in molar flux from 10^{10} to 38 · 10^{10} mol m^{-2} s^{-1} for AMPA. The decrease in removal and the increase in the rate of disappearance r_i'' of GLY and AMPA suggested that photocatalytic reaction kinetics were not limited by the surface reaction rate but rather by mass transfer and molar flux to the membrane surface. The increase in r_i'' of GLY with flux was more significant compared to AMPA at flux < 1500 L m^{-2} h^{-1}, likely due to the higher diffusivity of AMPA (9 · 10^{-10} m^2 s^{-1} at 23 °C) compared to GLY (7 · 10^{-10} m^2 s^{-1} at 23 °C),[129] allowing more AMPA to pass through the membrane.

At flux > 2000 L m^{-2} h^{-1} (hydraulic residence time < 0.2 s), GLY and AMPA removal stabilized at 10–15 ± 9% and 5–7 ± 4 %, respectively. GLY r_i'' increased from 10^{10} to 10 ± 3 · 10^{10} mol m^{-2} s^{-1}, while AMPA r_i'' increased to 12 ± 4 · 10^{10} mol m^{-2} s^{-1} at a flux of 3000 L m^{-2} h^{-1}. At low hydraulic residence times (< 0.2 s), degradation was controlled by the surface reaction rate, which was consistent with findings in other flow-through photocatalytic reactor studies.[127,130] To what extent the herbicide concentration determines this reaction rate will be investigated next.

2.5. Water Quality: GLY and AMPA Concentration

To investigate the extent to which the removal and degradation rates of GLY and AMPA are limited by their initial concentrations, photocatalysis was performed across a wide range of concentrations (0.1—10000 µg L^{-1}), which are environmentally relevant (**Figure 5**). The hydraulic residence time in these experiments is 0.5 s.

GLY and AMPA removal decreased (from 65 ± 6 to 5 ± 4% for GLY and from 82 ± 8 to 2 ± 2% for AMPA) as the feed concentration increased from 0.1 to 10 000 µg L^{-1} (Figure 5). The rate of disappearance (r_i'') for both GLY and AMPA rose from 0.4 ± 1 · 10^{10} to 4671 ± 597 · 10^{10} mol m^{-2} s^{-1} for GLY and from 1.1 ± 1 · 10^{10} to 2703 ± 373 · 10^{10} mol m^{-2} s^{-1} for AMPA with an increase in feed concentration. This linear increase in r_i'' was attributed to the higher initial concentration, resulting in greater surface coverage of the photocatalyst. Therefore, the amount of herbicide at the surface was a limiting factor for the photodegradation of GLY and AMPA by the PVDF-TiO_2 membrane.

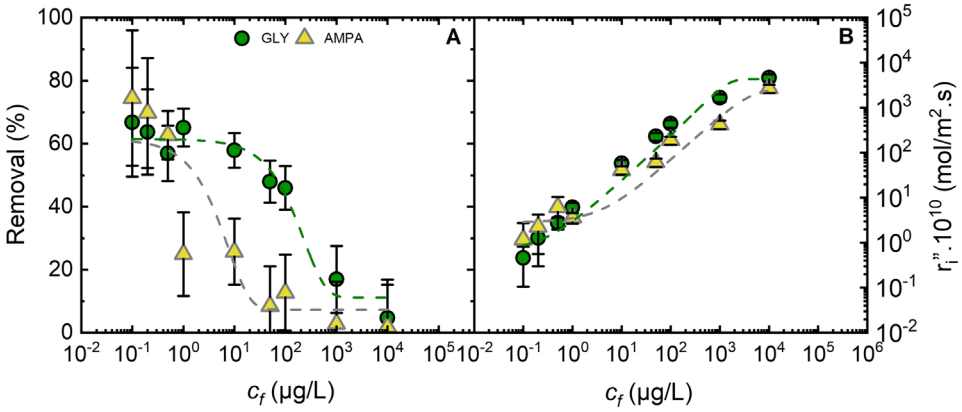

Figure 5. Removal (A) and rate of disappearance (r_i'') (B) of GLY/ AMPA under solar simulator at varied feed concentration (PVDF-TiO_2, J_w = 600 L m^{-2} h^{-1}, I (AM1.5 g 350–1150 nm) = 50 mW cm^{-2}, pH 8.1 ± 0.2, and 23 ± 1 °C). Dotted lines are guides for the eye.

At concentrations exceeding 1000 µg L^{-1}, the minimal removal of GLY and AMPA (2–5%) indicates that the PVDF-TiO_2 membrane has reached its limits of what can be degraded with the available ROS in the given time, even through r_i'' for both compounds continued to increase, reaching 4671 ± 597 · 10^{10} mol m^{-2} s^{-1} and 2703 ± 373 · 10^{10} mol m^{-2} s^{-1}, respectively. This indicates that degradation was still controlled by the feed concentration and thus the availability of micropollutant molecules in the photocatalytic membrane reactor, where mass transfer limitation was eliminated by the convective flow. Careful process design is required to ensure that both removal and the highest possible reaction rates ensure optimal performance. For water treatment applications, the high concentrations are not relevant for micropollutants, and results are clearly concentration dependent.

2.6. Water Quality: pH of GLY/AMPA Solution

The pH of the solution can influence the photocatalytic degradation of GLY and AMPA by altering speciation, surface interactions between GLY/AMPA and the catalysts, as well as affecting the concentration of ROS. To evaluate the extent to which pH-dependent interactions contribute to GLY and AMPA degradation, photocatalysis was investigated at varied initial pH ranging from 2 to 12 (**Figure 6**).

The removal of GLY and AMPA decreased drastically from 86 ± 3 to 4 ± 4% for GLY and from 51 ± 9 to 3 ± 3% for AMPA (Figure 6) as the pH increased from 2 to 12. This trend corresponds to a change in GLY charge from +0 to −3 and in AMPA charge from +0 to −2 (Table S2, Supporting Information). Meanwhile, r_i'' for GLY and AMPA decreased from 8 ± 2 · 10^{10} to 1 ± 0.2 · 10^{10} mol m^{-2} s^{-1}, and from 6 ± 2 · 10^{10} to 1 ± 0.2 · 10^{10} mol m^{-2} s^{-1}, respectively. TiO_2 has a point of zero charge (pH_{IEP}) at 3.3, with the negative charge at pH > 3.3.[131] Therefore, at low pH, GLY and AMPA could accumulate on the metal oxide surface (TiO_2 in this study) due to electrostatic attraction and adsorb on the TiO_2 surface.[132] The adsorption of GLY/AMPA at the dark phase showed that GLY and AMPA were adsorbed better at lower pH than at higher pH (Figure S18, Supporting Information). Functional groups, such as carboxyl and phosphonate, of the herbicides can form complexes and have hydrogen bonding with TiO_2.[122,123,133] At pH > 4, GLY and AMPA charges range from −1– −3, while TiO_2 is negatively charged, leading to electrostatic repulsion. Furthermore, an increase in pH enhances the competition of OH^- with complexation and hydrogen bonding, resulting in mononuclear monodentate complexes between

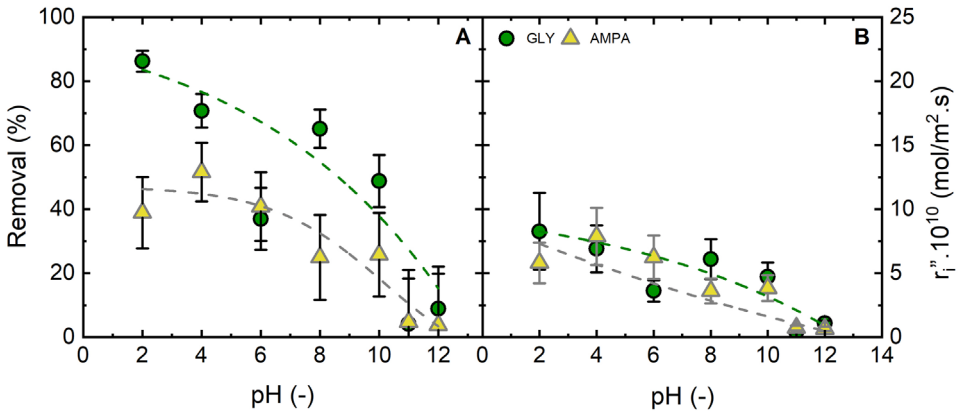

Figure 6. Removal (A) and rate of disappearance (r_i'') (B) of GLY/ AMPA under solar simulator at varied initial pH of feed solution (PVDF-TiO_2, c_f (GLY/AMPA) = 1 µg L^{-1}, J_w = 600 L m^{-2} h^{-1}, I (AM1.5 g 350–1150 nm) = 50 mW cm^{-2}, and 23 ± 1 °C). Dotted lines are guides for the eye.

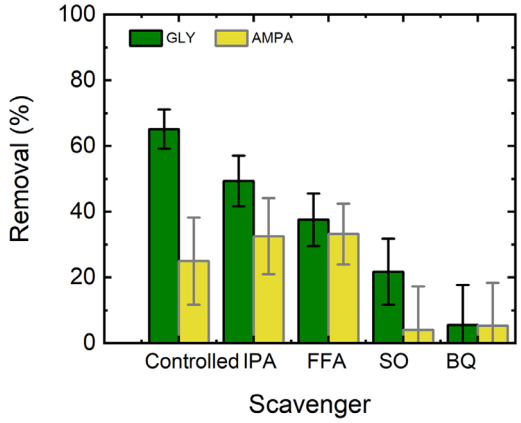

Figure 7. Removal of GLY/AMPA under solar simulator with varied types of scavengers (PVDF-TiO_2, c_f (GLY/AMPA) = 1 µg L^{-1}, J_w = 600 L m^{-2} h^{-1}, I (AM1.5 g 350–1150 nm) = 50 mW cm^{-2}, pH 8.1 ± 0.2, 23 ± 1 °C).

GLY/AMPA functional groups and Ti at high pH.[122,132] Consequently, lower adsorption onto TiO_2 results in decreased photocatalytic degradation of GLY and AMPA by the PVDF-TiO_2 membrane.

Moreover, different pH could affect ROS formation by changing the ROS concentration. The decreased removal at higher pH was also reported in other study, where acidic conditions were preferred for GLY photodegradation due to the formation of •OOH, a less reactive species.[73] In the study of Chen and Liu in batch experiments, GLY removal increased from 36% to 67% with the decrease of pH from neutral to acidic conditions, which was attributed to more ROS (•OH and $\bullet O_2^-$) formation.[73] At high pH, the concentration of scavengers such as CO_3^{2-} and HCO_3^- increases, leading to a decrease in ROS concentration available for GLY/AMPA photodegradation.[82]

Identifying the contributions of various ROS in the PVDF-TiO_2 membrane reactor is critical for a deeper understanding of the GLY/AMPA degradation mechanism, which will be investigated next by using different scavengers.

2.7. Identification of Predominant Reactive Oxygen Species in Degradation of GLY and AMPA

The role of key reactive species, including hydroxyl radical (•OH), superoxide radicals ($\bullet O_2^-$), singlet oxygen ($^1O_2$), valence band holes (h^+_{VB}), was determined through scavenging experiments, in which the contribution of each species to GLY/AMPA degradation was examined based on the inhibitory effects of the scavengers (**Figure 7**). The details about each scavenger and the target radicals are mentioned in Table S3 (Supporting Information).

With the •OH scavenger, isopropanol (IPA), the removal remained at 50 ± 8% for GLY and 32 ± 10% for AMPA (Figure 7). Therefore, •OH did not appear to contribute to degradation. This may be due to the scavenging effect of $NaHCO_3$ (rate constant 8.5 · 10^6 $M^{-1}s^{-1}$[134]) at a concentration (1 mM) that was six orders of magnitude higher than that of GLY/AMPA,[135] thereby inhibiting photodegradation.

The presence of furfuryl alcohol (FFA) reduced GLY removal from 65 ± 6 to 38 ± 8%, while AMPA removal remained unaffected. FFA reacts rapidly with $^1O_2$ ($k_{FFA,^1O_2} = 1.2 \cdot 10^8 M^{-1}s^{-1}$) with a high rate, and with $\bullet O_2^-$ with a lower rate ($k_{FFA,\bullet O_2^-} = 3.5 \cdot 10^3 M^{-1}s^{-1}$).[136] The reduced removal may be attributed to the scavenging of a small fraction of $\bullet O_2^-$ by FFA, making it difficult to clearly determine the role of $^1O_2$.

In the presence of sodium oxalate (SO), GLY and AMPA removal decreased from 65 ± 6 to 22 ± 10% and from 25 ± 11 to 4 ± 4%, respectively. This suggests that a portion of the adsorbed GLY/AMPA was directly degraded by h^+_{VB} at the catalyst surface, which explains the higher removal at lower pH corresponding to better adsorption on TiO_2 (Figure 6).

GLY and AMPA removal was completely inhibited by benzoquinone (BQ), with final removal of 6 ± 2% for GLY and 5 ± 2% for AMPA. This confirms that $\bullet O_2^-$ is the primary reactive species responsible for GLY/AMPA degradation and is expected to be the dominant at the higher concentration of GLY and AMPA due to the scavenging effect of $NaHCO_3$. However, the scavenging effect is strongly dependent on the concentration of GLY and AMPA.[137] The reaction rate of GLY and •OH is ≈10^{10} $M^{-1}s^{-1}$,[138] which is four orders of magnitude higher than that between •OH and HCO_3^-. The increase of GLY and AMPA concentration could lead to the stronger competition of GLY/AMPA for ROS compared to $NaHCO_3$, potentially shifting the reaction mechanisms, in which such concentrations are unrealistically high, and this case is not anticipated as a realistic option (in the range of mg/L).

Having identified the main reactive species, the degradation pathway of GLY and AMPA via the PVDF-TiO_2 membrane was further examined using computational chemistry calculations and bond dissociation enthalpy (BDE) analysis.

2.8. Determination of Bond Dissociation Enthalpy and Degradation Pathway

Since $\bullet O_2^-$ was identified as the dominant ROS for GLY/AMPA degradation (Figure 7), the final step in explaining the photodegradation was to determine potential radical attack points on GLY and AMPA molecules to understand their degradation pathways. To achieve this, the X—H (where X can be C, N, or O) and X—Y (where X and Y can be P, C, N, or O) homolytic bond dissociation enthalpies (BDEs) were calculated for each unique bond (**Figure 8**).

By comparing BDE, the relative strength of the corresponding bonds was determined. The higher BDE show the stronger bonds, and the weakest points of the structure have the lowest BDE. In GLY, the weakest C—H bond is located between the amine and carboxyl groups, with a BDE of 419.2 kJ mol^{-1}. In AMPA, the weakest X—H bond is the only C—H bond in the structure with a BDE value of 431.7 kJ mol^{-1}, similar to the corresponding bond in GLY (Figure 8). The weakest X—Y bond in GLY is the C—N bond with a BDE of only 328.8 kJ mol^{-1}. This bond is weaker than the C—H bonds, making it more prone to breaking. Therefore, the bond between the amine group and the carboxylate group in the GLY molecule is broken, forming AMPA as a degradation product and an additional side product, as observed in photodegradation experiments (Figure 2).

BDE maps alone are not able to provide a complete description of the degradation process, but can indicate where the

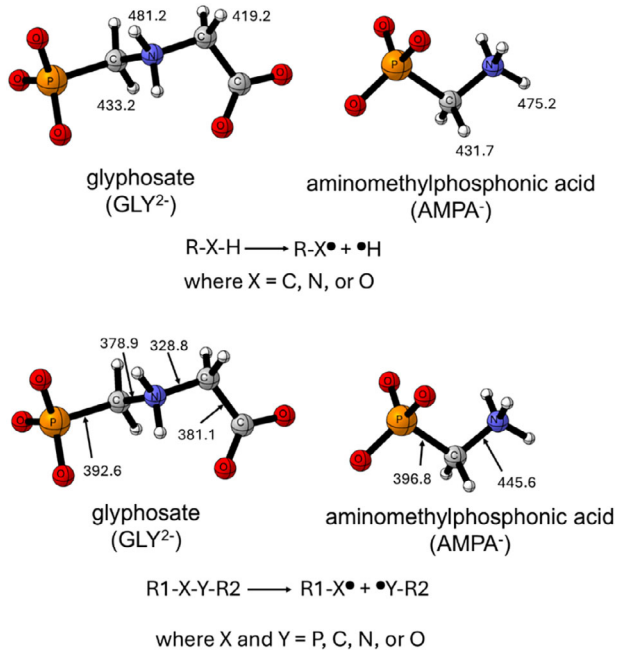

Figure 8. BDE (in kJ/mol) maps of GLY and AMPA at their most probable protonation state. Thermodynamic properties of the species and the corresponding radicals were determined by using the G3MP2B3 composite level of theory. BDE values (in kJ/mol) calculated by using the depicted equations for all unique bonds. The protonation states of the species were considered according to the experimental condition (pH 8), and thus, the charge of GLY and AMPA is −2 and −1, respectively.

degradation is most likely to start. Therefore, in addition to BDE values, secondary radical reactions, intramolecular rearrangements, and other factors must be considered. Based on the BDE analysis, which identified the most vulnerable bonds, a probable degradation pathway for GLY/AMPA via $\bullet O_2^-$ (**Figure 9**) was proposed using G3MP2B3 calculations, experimental data, and analysis of previously published studies.[110,139]

As the BDE map and previous studies revealed,[110] the C—H bond located between the amine and carboxyl groups of GLY is the most susceptible to $\bullet O_2^-$ attack. The feasible reaction mechanism for GLY degradation and AMPA formation in the presence of superoxide radicals was computed. A $GLY^{2-}\bullet$ radical was formed (Figure 9, top), which is one of the most favored processes in case the degradation starts with hydrogen abstraction. In the next step, superoxide radical can form a stable non-radical adduct with the $GLY^{2-}\bullet$ radical (Figure 9, middle) via a thermodynamically favored process. Subsequent intramolecular rearrangement leads to the formation of a stable AMPA and oxalic acid (Figure 9, bottom). It is important to note that metabolite identification was not part of this study, which would be incredibly difficult at realistic concentrations.

2.9. Enhanced Photocatalytic Degradation at Optimized Conditions

To determine whether solar-activated PVDF-TiO_2 can achieve the guideline limit of 0.1 µg L^{-1} for both GLY and AMPA in water intended for domestic consumption, photocatalysis was performed under optimized conditions, considering both removal efficiency and r_i'' (flux of 60 L m^{-2} h^{-1} and simulated solar irradiance of 98 mW cm^{-2}) (**Figure 10**).

The optimized conditions corresponded to a flux of 60 L m^{-2} h^{-1}, equivalent to a hydraulic residence time of 4.5 s, under solar irradiance of 98 mW cm^{-2}. The permeate concentration of GLY was 0.04 ± 0.03 µg L^{-1}, satisfying the EU guideline for individual herbicides (0.1 µg L^{-1}).[23] However, AMPA did not meet this guideline, as the permeate concentration was 0.2 ± 0.04 µg L^{-1} (Figure 10). This would require a higher light intensity or indeed a UV light source. The total permeate concentration of GLY and AMPA (0.3 ± 0.04 µg L^{-1}) was below the EU guideline for total herbicides (0.5 µg L^{-1}),[23] even though this is an ideal situation in a synthetic background solution. Results highlight that photocatalytic degradation using the PVDF-TiO_2 membrane in a flow-through configuration can remove GLY and AMPA from water, while further research to enhance AMPA removal and build resilience in real waters needs to be addressed.

3. Conclusion

The photocatalytic degradation of GLY and AMPA was investigated using a PVDF-TiO_2 membrane under simulated solar irradiation in a continuous flow-through operation. The degradation efficiency of GLY and AMPA under solar spectrum irradiation (AM1.5G, 350–1150 nm) was comparable to that under UV light (365 nm) at equivalent absorbed irradiance (65 ± 6% for GLY and 25 ± 6% for AMPA removal). Non-UV wavelengths did not contribute to the degradation of GLY and AMPA, indicating that degradation was entirely driven by the UV spectrum.

To identify limiting factors, photocatalytic experiments were conducted under varying irradiance, flux, concentration, and pH. GLY removal significantly increased to ≈80% under elevated solar irradiance (90 mW cm^{-2}), confirming that light irradiance is a limiting factor in GLY/AMPA degradation. At high irradiance (>70 mW cm^{-2}), incomplete removal (79 ± 4%) at a stable rate of disappearance r_i'' ($8 \pm 2 \cdot 10^{10}$ mol m^{-2} s^{-1}) suggested that mass transfer limitations played a role, as also observed in filtration experiments with varying initial concentrations. Maximum adsorption was reached at the highest herbicide concentration, inhibiting photodegradation, suggesting that micropollutant availability in the photocatalytic membrane reactor is a key controlling factor. GLY and AMPA removal decreased with increasing pH, correlating with TiO_2 adsorption behavior and ROS formation. At higher pH, GLY/AMPA adsorption onto TiO_2 decreased, lowering photocatalytic degradation. Furthermore, higher pH also increased the concentration of scavenger radicals such as CO_3^{2-} and HCO_3^-, reducing ROS availability. $\bullet O_2^-$ and h_{VB}^+ appear to be the primary species contributing to the removal of GLY/AMPA in which $\bullet O_2^-$ concentration would be controlled by solar irradiance and solution pH.

In the photocatalytic degradation experiments, GLY was degraded more efficiently than AMPA, which was attributed by i) GLY being intrinsically more degradable than AMPA; ii) AMPA being formed as an intermediate during GLY degradation. The formation of AMPA during GLY photodegradation was confirmed in individual degradation experiments. Moreover, BDE calculations indicated that C—N bond cleavage was the preferred

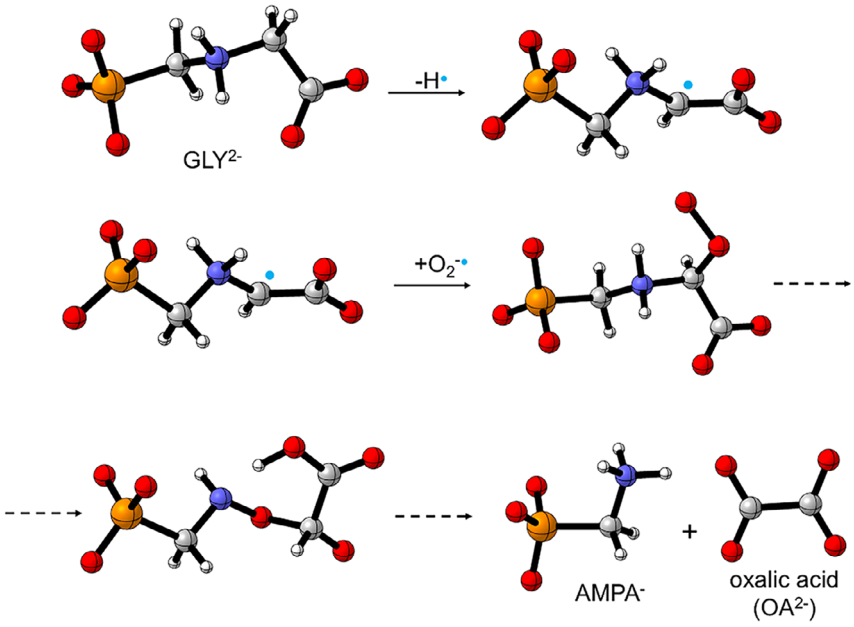

Figure 9. Probable glyphosate (GLY^{2-}) degradation pathway to $AMPA^{-}$ and oxalic acid.

degradation pathway in GLY, leading to AMPA as the main degradation product.

4. Experimental Section

Photocatalytic Filtration System and Protocol: The membrane photocatalysis experiments were conducted using a custom-built micro cross-flow system (**Figure 11**; Figure S19, Supporting Information). Further details of this setup and its comprehensive hydrodynamic characterization have been reported in previous work.[127,140]

The membrane cell consists of a stainless steel module (or microreactor) with an active membrane area of 2 cm^2, a channel height of 0.7 mm, and a quartz window (active illumination area: 2 cm^2, Zell Quarzglas, Germany). A high-pressure pump (Pump 80P, pump head 500 mL SST, KNAUER Wissenschaftliche Geräte GmbH, Germany) was used.

A UV LED (M365LP1, peak wavelength: 365 nm, Thorlabs, USA) with an LED driver (DC2200, Thorlabs) served as the UV light source, as described in a previous study.[127] A solar simulator (SINUS-70, wavelength range: 350—1150 nm, WAVELABS Solar Metrology Systems GmbH, Germany) provided a broad range of light wavelengths (Figure S13, Supporting Information).

The system was equipped with the feed pressure sensors (WIKA S-10, 0–1 bar; WIKA A-10, 0–40 bar, Germany), a permeate pressure sensor (WIKA S-10, 0–1 bar, Germany), and a permeate in-line conductivity sensor (ET131, eDAQ, Australia). A water chiller (Minichiller 300 OLÉ, Peter Huber Kältemaschinenbau, Germany) was used to control and maintain the feed temperature, while a 16-port switching valve (Azura V2.1S, Knauer) was used to collect multiple samples automatically. The system was connected to a computer running LabVIEW software (Version 14.0.1, National Instruments, Germany) for automated control of the switching valve, feed flow rate, time, and light intensity for the UV LED. The solar simulator was controlled by SinusGUI v2.5 (Wavelabs, USA). Experimental parameters, including pressure, temperature, conductivity, and permeate mass, were

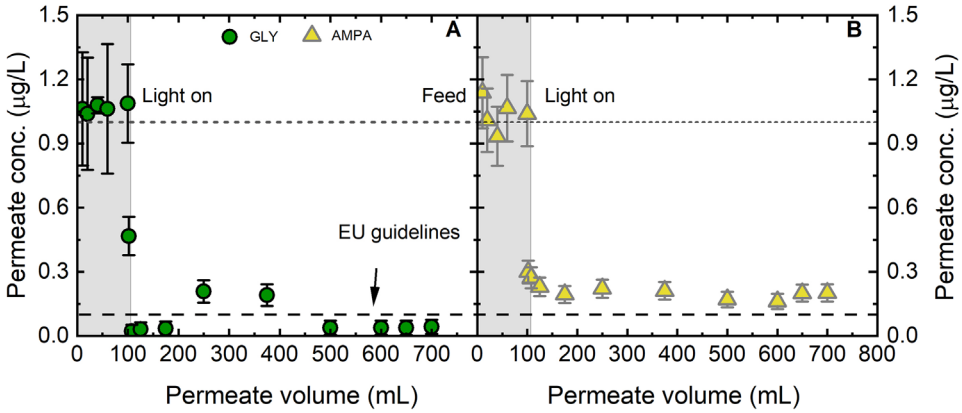

Figure 10. Permeate concentration of GLY (A) and AMPA (B) versus permeate volume at optimized conditions (PVDF-TiO_2, c_f (GLY/AMPA) = 1 µg L^{-1}, J_w = 60 L m^{-2} h^{-1}, I (AM1.5 g 350–1150 nm) = 98 mW cm^{-2}, pH 8.1 ± 0.2, 23 ± 1 °C).

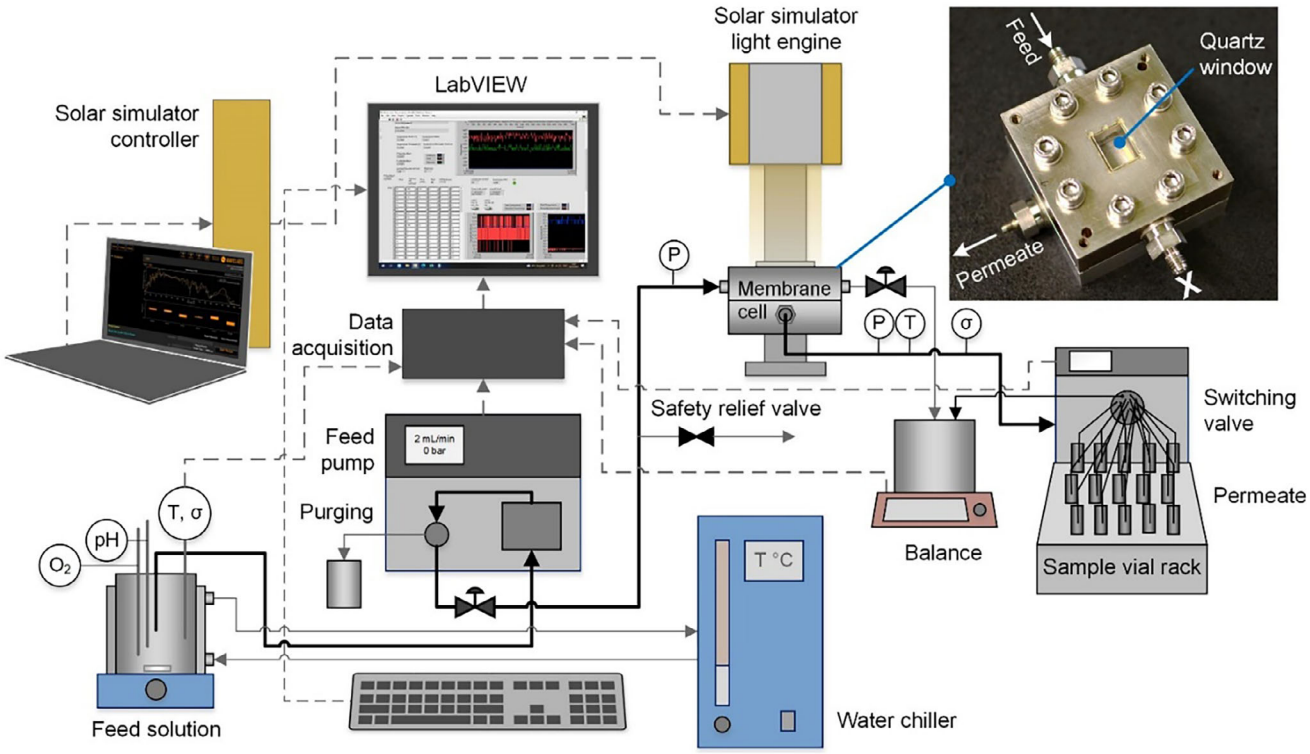

Figure 11. Schematic illustration of the membrane photocatalysis set-up and the photograph (inset) of the photocatalytic membrane cell with a dead-end configuration (retentate valve closed). The system is equipped with pressure P, temperature T, conductivity σ, pH, and dissolved oxygen O_2 sensors.

monitored via a data acquisition card (USB-6000, National Instruments, USA).

All photocatalytic filtration experiments were performed in a flow-through dead-end configuration with the retentate valve closed. The photocatalytic filtration protocol is summarised in Table S4 (Supporting Information), adapted from previous work[91] with different light sources and corresponding parameter settings. Either UV light (365 nm) or a solar simulator (AM1.5G, 350—1150 nm) was used, and photophysical properties are compared with TiO_2 in Table S5 (Supporting Information). To quantify adsorption, photocatalysis was conducted after the dark-phase filtration reached equilibrium, while photolysis was determined using a pristine membrane (in the absence of photocatalyst). Operational parameters were shown in Table S1 (Supporting Information).

Photocatalytic Membranes: The membrane used was a PVDF-TiO_2 membrane prepared and supplied by the Institute of Surface Engineering (IOM), Leipzig, the preparation method and membrane characteristics were previously described by Fischer et al. .[127,141] In brief, the TiO_2 nanoparticle (NPs) suspension was prepared by mixing 4 mL of titanium (IV) isopropoxide (TTIP) with 80 mL of 0.1 M HCl and stirred for 15 min at room temperature. The mixture solution was then heated in a pressure vessel at 210 °C for 20 h, cooled, and subsequently dispersed using an ultrasonic probe for 90 s at 40 W (Sonoplus, HD2200 Generator, KE76 probe, BANDELIN electronic GmbH & Co. KG, Berlin, Germany). A standard PVDF membrane (0.22 µm, Millipore, USA) (90 mm × 90 mm) was then placed (with the active layer facing downwards) into the suspension and shaken for 5 min. The membrane was subsequently washed with Milli-Q water and dried at 100 °C for 30 min. The PVDF-TiO_2 membrane contained 5.2 ± 0.2% TiO_2 on the membrane surface with the pore size of 0.22 µm[127] with the membrane thickness of $1.25 \cdot 10^{-4}$ m, porosity of 0.6.[142]

Micropollutants and Solution Chemistry: Details about solution preparation have been reported in previous work.[28] The Stock 1 (GLY and AMPA mixture solution) was prepared by dissolving both GLY (Sigma Aldrich, 98%) and AMPA powder (Sigma–Aldrich, 99%) in Milli-Q water with a concentration of 10 mg L^{-1} for each compound (the properties summarised in Table S4, Supporting Information). Stock 2 (GLY/AMPA at a concentration of 100 µg L^{-1} for each compound) was prepared by diluting Stock 1 in Milli-Q water. Feed solutions of environmentally relevant GLY/AMPA concentrations (0.1–50 µg L^{-1}) were prepared by diluting Stock 2 in background electrolyte solutions. A higher concentration of GLY/AMPA (1 mg L^{-1}) was prepared by directly diluting Stock 1 in background electrolyte solutions. Experiments were carried out with a mixture of GLY and AMPA at the indicated concentration of each in the mixture; hence, the feed solution contained 1 µg L^{-1} of GLY and 1 µg L^{-1} of AMPA in all experiments except for experiments with variable feed concentration. For experiments of individual herbicides, a stock solution and a feed solution containing the individual herbicide at the same concentration as in a mixture were used. All feed solutions were prepared in background electrolytes of 1 mM $NaHCO_3$ and 10 mM NaCl to simulate the real water matrixes.[143] The background electrolyte stock solution was prepared daily from 100 mM $NaHCO_3$ (dissolved from analytical-grade, >99.7% powder, Merck, Germany) and 1 M NaCl (dissolved from analytical-grade ≥99.5% powder, Honeywell Fluka, Germany) in Milli-Q water (Reference A+, Merck Millipore, USA). The conductivity and pH of the background solution were ≈1400 µS cm^{-1} and 8.1 ± 0.2, unless adjusted with 1 M HCl (diluted from 37% HCl, Roth, Germany) and 1 M NaOH (dissolved from pellets, Merck, 99%) for pH experiments. Analytical standards (analytical-grade, 100 mg L^{-1} in Milli-Q water) of GLY and AMPA were obtained from Dr. Ehrenstorfer (Germany) for analysis and quality control of the analysis. ^{13}C GLY (analytical grade, 98%, Sigma Aldrich, USA) was used as the internal standard for analysis, and ammonium formate powder (analytical-grade, 99%, VWR, Germany) was used as a buffer for analysis.

Analytical Methods: GLY and AMPA were quantified using liquid chromatography with tandem mass spectrometry (LC-MS/MS), which consisted of an ultra-high-performance liquid chromatographic (UHPLC)

system (LX50) coupled to a QSight 420 triple-quadrupole mass spectrometer (PerkinElmer, USA). Details regarding the analytical method have been reported in previous work.[144] The hydrophilic interaction liquid chromatography (HILIC) column used was an Obelisc N (2.1 × 150 mm, 5 µm, SIELC Technologies, USA), through which an isocratic mobile phase of 85/15 v/v (H_2O: acetonitrile + 0.05% CH_2O_2) was eluted. In the mass spectrometer (MS), electrospray ionization (ESI) was employed in negative mode, with a source temperature of 450 °C and a hot surface-induced desolvation (HSID) temperature of 320 °C (Table S6, Supporting Information). 10 µL of internal standard (^{13}C GLY 100 µg L^{-1}) and 10 µL of buffer (ammonium formate 200 mM) were added to each 1000 µL of sample or standard. 100 µL of the prepared sample or standard was injected into LC-MS/MS, with a mobile phase flow rate of 0.6 mL min^{-1}. The concentrations of GLY and AMPA were calculated based on calibration solutions prepared at 10, 20, 50, 200, 500, and 1000 ng L^{-1}. The determined detection limit was 10 ng L^{-1} (Figure S19,S20, Supporting Information). Data analysis was carried out using the Simplicity 3Q software platform. Dissolved oxygen in the feed solution for each experiment was measured using a multi-parameter measuring device (MultiLine 3620 IDS, WTW, Germany), equipped with an optical DO sensor (FDO 925, WTW, Germany).

Identification of Reactive Oxygen Species: The predominant ROS contributing to the degradation of GLY and AMPA were determined using scavenging experiments, of which the principle rely on the distinct reactivity between different reactive species and specific scavenger.[145] In the scavenging experiments, a 10 mM scavenger solution was added to the feed solution before initiating photocatalytic filtration. Different scavengers were used to identify the contributions of various ROS: isopropanol (IPA, > 99.8%, HPLC grade, VWR, Germany) – for hydroxyl radical (•OH); p-Benzoquinone (p-BQ, > 98%) – for superoxide radicals ($\bullet O_2^-$); furfuryl alcohol (FFA, 98%) – for singlet oxygen ($^1O_2$); sodium oxalate (SO, 99%) for valence band holes (h^+_{VB}), all from Thermo Scientific Chemicals, Germany. The scavenger and their rate constants are summarised in Table S3 (Supporting Information).

Computational Chemistry Calculations of GLY and AMPA: The 3D starting structures of GLY and AMPA were prepared using GaussView 6 software.[146] The protonation states were determined based on the experimental conditions (pH 8), where the dominant species had charges of −2 for GLY and −1 for AMPA. Additional calculations were performed for the neutral, monoanionic GLY, and zwitterionic AMPA species. The thermochemical properties of the structures were determined using the G3MP2B3 composite method,[116,117] implemented in the Gaussian 16 (Revision C.01) program package. Geometry optimizations and frequency calculations were conducted at the B3LYP/6-31G(d) level of theory as part of the G3MP2B3 protocol. Single-point energy calculations at the QCISD(FC,T)/6-31G(d) and MP2(FC)/G3MP2Large levels of theory were also performed as part of the G3MP2B3 composite scheme. Solvent effects were modeled using the SMD model to account for water as the solvent.[147] Based on the optimised AMPA and GLY structures, the corresponding unique radical species were prepared by removing one hydrogen atom at a time from the structures (X—H, where X can be C, N, or O) or breaking X—Y bonds (where X and Y can be P, C, N, or O) and creating two radical species from the optimized structures. The thermochemical properties of such prepared radical structures were calculated using the above-described G3MP2B3 composite method, which was successfully applied to radicals and other similar systems.[148]

To compare the preference of radical formation and identify potential radical attack points on the structures, homolytic bond dissociation enthalpies (BDEs) were determined by using the corresponding calculated enthalpy values of each studied species and using them to determine the enthalpy change of the following reactions;

$$R - X - H \rightarrow R - X^{\bullet} + H^{\bullet} \quad (2)$$

$$R_1 - X - Y - R_2 \rightarrow R_1 - X^{\bullet} + R_2 - Y^{\bullet} \quad (3)$$

Thus, $BDE_{X\text{-}H}$ and $BDE_{X\text{-}Y}$ were determined by calculating the corresponding reaction enthalpies of the above bond-breaking reactions as follows;

$$BDE_{X-H} = \Delta H_{X-H} = H_{R-X^*} + H_{H^*} - H_{R-X-H} \quad (4)$$

while

$$BDE_{X-Y} = \Delta H_{X-Y} = (H_{R_1-X^*} + H_{R_2-Y^*}) - H_{R_1-X-Y-R_2} \quad (5)$$

The BDE values were compared to determine the most likely radical attack points. In each case, a homolytic cleavage of a single bond in isolation was considered. However, the degradation of species typically involves multistep procedures involving rearrangements, secondary radical reactions, and others, which cannot be captured by a single BDE value. Therefore, a bond dissociation enthalpy map alone was not suitable to provide a complete picture of the degradation. Thus, additional calculations were conducted based on the structures of the most feasible radical species, experimental considerations of this work, and literature data.[110,139] By integrating these factors, a potential superoxide radical attack pathway for GLY was proposed. The corresponding structures were generated, optimized, and analyzed using the Gaussian 16 (Revision C.01) program package.[149]

Data Analysis: The removal and rate of disappearance (r_i'') were the primary parameters used to evaluate the performance of the PVDF-TiO_2 membrane (summarized in Table S7, Supporting Information). Error propagation was estimated by considering uncertainties from solution preparation, analytical instruments, and the photocatalytic filtration system.[150] The most significant source of error was from analytical inaccuracies (see Tables S8–S10, Supporting Information). The reproducibility of GLY and AMPA photocatalytic degradation was examined by performing five repetitions of photocatalytic filtration experiments using UV light at an irradiance of 10 mW cm^{-2} (Figure S21, Supporting Information).

Supporting Information

Supporting Information is available from the Wiley Online Library or from the author.

Acknowledgements

The Helmholtz Recruitment Initiative is thanked for the IAMT laboratory and project funding. Deutscher Akademischer Austauschdienst (DAAD) provided a PhD scholarship for P.B.T (program ID 57440921) and N.F.H. The Bundesministerium für Bildung und Forschung (BMBF) project NEMWARE is thanked for project funding (02WIL1555, A.I.S) in collaboration with Prof Daniel Mandler (HUIJ, Israel) and Prof Rafael Semiat (Technion, Israel). The authors acknowledge the Digital Government Development and Project Management Ltd. for awarding us access to the Komondor HPC facility based in Hungary. BF thanks the support by the János Bolyai Research Scholarship of the Hungarian Academy of Sciences. Calculations have also been carried out using resources provided by Wroclaw Center for Networking and Supercomputing (http://wcss.pl). Dr Kristina Fischer and Dr Agnes Schulze (IOM Leipzig, Germany) are thanked for membrane modification and provision of TiO_2-coated membranes and the continued collaboration. Prof Babak Minofar (University of Lodz, Poland) is thanked for the discussion on bond dissociation enthalpy and degradation pathways. Dr Minh Nguyen (KIT-IAMT) contributed ideas on quenching of degradation and photocatalytic degradation mechanism, while Prof Bryce Richards (MIT-IMT) has provided the solar simulator methodology and ongoing collaboration with photocatalysis. Open access publication is supported by the DEAL agreement.

Open access funding enabled and organized by Projekt DEAL.

Conflict of Interest

The authors declare no conflict of interest.

Data Availability Statement

The data that support the findings of this study are available from the corresponding author upon reasonable request.

Keywords

advanced oxidation processes, herbicides, membrane process, organophosphates, photodegradation, physio-chemical water treatment

Received: May 7, 2025
Revised: October 13, 2025
Published online:

[1] D. Soares, L. Silva, S. Duarte, A. Pena, A. Pereira, *Foods* **2021**, *10*, 2785.
[2] J. P. Giesy, S. Dobson, K. R. Solomon, in *Reviews of Environmental Contamination and Toxicology: Continuation of Residue Reviews* (Ed.: G.W. Ware), Springer, New York, **2000**, pp. 35-120.
[3] Y. Chen, W.-J. Chen, Y. Huang, J. Li, J. Zhong, W. Zhang, Y. Zou, S. Mishra, P. Bhatt, S. Chen, *Environ. Res.* **2022**, *215*, 114153.
[4] R. Annett, H. R. Habibi, A. Hontela, *J. Appl. Toxicol.* **2014**, *34*, 458.
[5] E. Okada, M. Allinson, M. P. Barral, B. Clarke, G. Allinson, *Water Res.* **2020**, *168*, 115139.
[6] S. R. Moller, A. F. Wallace, R. Zahir, A. Quadery, D. P. Jaisi, *J. Hazard. Mater.* **2024**, *461*, 132467.
[7] S. R. Moller, M. A. Campos, J. I. Rilling, R. Bakkour, A. J. Hollenback, M. A. Jorquera, D. P. Jaisi, *J. Hazard. Mater.* **2024**, *477*, 135238.
[8] V. J. Koller, M. Fürhacker, A. Nersesyan, M. Mišík, M. Eisenbauer, S. Knasmueller, *Arch. Toxicol.* **2012**, *86*, 805.
[9] K. Z. Guyton, D. Loomis, Y. Grosse, F. El Ghissassi, L. Benbrahim-Tallaa, N. Guha, C. Scoccianti, H. Mattock, K. Straif, *Lancet Oncol.* **2015**, *16*, 490.
[10] J. P. Myers, M. N. Antoniou, B. Blumberg, L. Carroll, T. Colborn, L. G. Everett, M. Hansen, P. J. Landrigan, B. P. Lanphear, R. Mesnage, L. N. Vandenberg, F. S. vom Saal, W. V. Welshons, C. M. Benbrook, *Environ. Health* **2016**, *15*, 19.
[11] C. Nerozzi, S. Recuero, G. Galeati, D. Bucci, M. Spinaci, M. Yeste, *Sci. Rep.* **2020**, *10*, 11026.
[12] H. Fingerhut, D. A. Lieb, Bayer backs broadened effort to shield popular weedkiller from claims it failed to warn of cancer, Jefferson City, Missouri, https://apnews.com/article/bayer-roundup-glyphosate-pesticide-liability-cancer-7d7885e55e228fae8ed8ec7b207a65b8 (accessed: March 2025).
[13] M. Schwientek, H. Rügner, S. B. Haderlein, W. Schulz, B. Wimmer, L. Engelbart, S. Bieger, C. Huhn, *Water Res.* **2024**, *263*, 122140.
[14] A. Connolly, H. M. Koch, *Environ. Health Perspect.* **2023**, *131*, 71304.
[15] R. Finger, N. Möhring, P. Kudsk, *Commun. Earth Environ.* **2023**, *4*, 286.
[16] B. Casassus, *Nature* **2023**, 2023.
[17] European Commission, Renewal of the approval of glyphosate: Questions and Answers, **2023**, https://ec.europa.eu/commission/presscorner/api/files/document/print/en/qanda_23_5793/QANDA_23_5793_EN.pdf (accessed: February 2025).
[18] C. A. Villamar-Ayala, J. V. Carrera-Cevallos, R. Vasquez-Medrano, P. J. Espinoza-Montero, *Crit. Rev. Environ. Sci. Technol.* **2019**, *49*, 1476.
[19] J. P. Muñoz, E. Silva-Pavez, D. Carrillo-Beltrán, G. M. Calaf, *Environ. Res.* **2023**, *231*, 116201.
[20] N. Suciu, E. Russo, M. Calliera, G. P. Luciani, M. Trevisan, E. Capri, *Sci. Total Environ.* **2023**, *866*, 161171.
[21] M. Feltracco, E. Barbaro, E. Morabito, R. Zangrando, R. Piazza, C. Barbante, A. Gambaro, *Environ. Sci. Pollut. Res.* **2022**, *29*, 16383.
[22] N. Tauchnitz, F. Kurzius, H. Rupp, G. Schmidt, B. Hauser, M. Schrödter, R. Meissner, *Environ. Pollut.* **2020**, *267*, 115186.
[23] The European Parliament and the Council of European Union, Directive (EU) 2020/2184 of the European parliament and of the council of 16 December 2020 on the quality of water intended for human consumption, in, Official Journal of the European Union, **2020**, pp. 37–38.
[24] S. Paul, W. F. Meggitt, P. Donald, *Weed Sci.* **1975**, *23*, 229.
[25] Z. W. Windom, M. Datta, M. M. Huda, M. A. Sabuj, N. Rai, *J. Mol. Liq.* **2022**, *365*, 120154.
[26] J. Gasperi, B. Laborie, V. Rocher, *Chem. Eng. J.* **2012**, *212*, 293.
[27] A. D. Villalobos-Lara, F. F. Rivera, J. Paramo-Vargas, Z. Gamiño-Arroyo, T. Ruiz-Vera, *J. Environ. Chem. Eng.* **2023**, *11*, 111214.
[28] P. B. Trinh, A. I. Schäfer, *Water Res.* **2024**, *250*, 121021.
[29] P. Yu, X. Li, X. Zhang, H. Zhou, Y. Xu, Y. Sun, H. Zheng, *Sep. Purif. Technol.* **2021**, *254*, 117662.
[30] G. A. Dissanayake Herath, L. S. Poh, W. J. Ng, *Chemosphere* **2019**, *227*, 533.
[31] W. Meng, X. Li, J. Yu, C. Xiao, H. Hou, R. Chi, G. Feng, *Environ. Sci. Pollut. Res.* **2023**, *30*, 57410.
[32] J. C. Diel, D. S. P. Franco, I. d. S. Nunes, H. A. Pereira, K. S. Moreira, T. A. de, L. Burgo, E. L. Foletto, G. L. Dotto, *J. Environ. Chem. Eng.* **2021**, *9*, 105178.
[33] G. Xiao, R. Wen, *Fluid Phase Equilib.* **2016**, *411*, 1.
[34] Y. Tao, F. Fang, Q. Lv, W. Qin, X. He, Y. Zhang, Y. Zhou, X. Li, J. Li, *J. Environ. Manage.* **2022**, *316*, 115301.
[35] S. Naghdi, E. Brown, M. Zendehbad, A. Duong, W. Ipsmiller, S. Biswas, M. C. Toroker, H. Kazemian, D. Eder, *Adv. Funct. Mater.* **2023**, *33*, 2213862.
[36] H. Park, A. May, L. Portilla, H. Dietrich, F. Münch, T. Rejek, M. Sarcletti, L. Banspach, D. Zahn, M. Halik, *Nat. Sustain.* **2020**, *3*, 129.
[37] D. A. Gkika, A. C. Mitropoulos, G. Z. Kyzas, *Sci. Total Environ.* **2022**, *822*, 153612.
[38] H. Saitúa, F. Giannini, A. P. Padilla, *J. Hazard. Mater.* **2012**, *227-228*, 204.
[39] J. Yuan, J. Duan, C. P. Saint, D. Mulcahy, *Environ. Technol.* **2018**, *39*, 1384.
[40] A. Loi-Brügger, S. Panglisch, G. Hoffmann, P. Buchta, R. Gimbel, C. J. Nacke, *Water Supply* **2008**, *8*, 85.
[41] M. A. Álvarez Bayona, A. Maturana Córdoba, R. J. Gallardo Amaya, A. M. Acevedo, *Front. Environ. Sci.* **2022**, *10*, 941836.
[42] W. Guo, H.-H. Ngo, J. Li, *Bioresour. Technol.* **2012**, *122*, 27.
[43] B. Díez, R. Rosal, *Nanotechnol. Environ. Eng.* **2020**, *5*, 15.
[44] A. Subramani, J. G. Jacangelo, *Sep. Purif. Technol.* **2014**, *122*, 472.
[45] M. Priyadarshini, I. Das, M. M. Ghangrekar, L. Blaney, *J. Environ. Manage.* **2022**, *316*, 115295.
[46] M. R. Assalin, S. G. De Moraes, S. C. N. Queiroz, V. L. Ferracini, N. Duran, *J. Environ. Sci. Health, Part B* **2009**, *45*, 89.
[47] L. Chen, S. Zhou, Y. Xu, Y. Sun, H. Zheng, *Desalin. Water Treat.* **2020**, *204*, 377.
[48] Y. Chen, F. Wu, Y. Lin, N. Deng, N. Bazhin, E. Glebov, *J. Hazard. Mater.* **2007**, *148*, 360.
[49] Y. Yang, Q. Deng, W. Yan, C. Jing, Y. Zhang, *Chem. Eng. J.* **2018**, *352*, 581.
[50] D. Chen, R. Zhao, H. Liu, H. Tian, Y. Tian, D. Huang, D. Johnson, Y. Huang, *J. Cleaner Prod.* **2025**, *491*, 144837.
[51] M. H. Tran, H. C. Nguyen, T. S. Le, V. A. D. Dang, T. H. Cao, C. K. Le, T. D. Dang, *Environ. Technol.* **2021**, *42*, 1155.
[52] Y. Xie, R. Xiong, J. Li, W. Li, X. Yang, H. Tong, *J. Environ. Manage.* **2023**, *333*, 117428.

[53] N. Tran, P. Drogui, T. L. Doan, T. S. Le, H. C. Nguyen, *Environ. Technol.* **2017**, *38*, 2939.
[54] U. von Gunten, *Environ. Sci. Technol.* **2018**, *52*, 5062.
[55] M. N. Chong, B. Jin, C. W. K. Chow, C. Saint, *Water Res.* **2010**, *44*, 2997.
[56] F.-Y. Chen, Z.-Y. Wu, Z. Adler, H. Wang, *Joule* **2021**, *5*, 1704.
[57] T. F. Qahtan, T. O. Owolabi, O. E. Olubi, A. Hezam, *Coord. Chem. Rev.* **2023**, *492*, 215276.
[58] H. Chen, S. Chen, X. Quan, Y. Zhang, *Environ. Sci. Technol.* **2010**, *44*, 451.
[59] J. Schneider, M. Matsuoka, M. Takeuchi, J. Zhang, Y. Horiuchi, M. Anpo, D. W. Bahnemann, *Chem. Rev.* **2014**, *114*, 9919.
[60] A. L. Linsebigler, G. Lu, J. T. Yates, Jr., *Chem. Rev.* **1995**, *95*, 735.
[61] P. Garcia-Muñoz, W. Dachtler, B. Altmayer, R. Schulz, D. Robert, F. Seitz, R. Rosenfeldt, N. Keller, *Chem. Eng. J.* **2020**, *384*, 123315.
[62] I. R. Verdi, A. J. Maroli Neto, I. S. D. G. Garcia, G. G. Lenzi, M. A. Villetti, O. C. Alves, M. Z. Fidelis, R. D. C. Rocha, R. Brackmann, *Mater. Sci. Semicond. Process.* **2024**, *174*, 108205.
[63] Y. Zhang, H. Cao, J. Lu, Y. Li, M. Bao, *J. Colloid Interface Sci.* **2022**, *607*, 607.
[64] Y. Chen, Y. Huang, H. Tian, L. Ye, R. Li, C. Chen, Z. Dai, D. Huang, *J. Environ. Sci.* **2023**, *127*, 60.
[65] J. M. Montiel-León, G. Munoz, S. Vo Duy, D. T. Do, M.-A. Vaudreuil, K. Goeury, F. Guillemette, M. Amyot, S. Sauvé, *Environ. Pollut.* **2019**, *250*, 29.
[66] Y. Geng, L. Jiang, D. Zhang, B. Liu, J. Zhang, H. Cheng, L. Wang, Y. Peng, Y. Wang, Y. Zhao, Y. Xu, X. Liu, *Sci. Total Environ.* **2021**, *769*, 144396.
[67] R. Lyubimenko, O. I. Gutierrez Cardenas, A. Turshatov, B. S. Richards, A. I. Schäfer, *Appl. Catal., B* **2021**, *291*, 120097.
[68] S. Banerjee, S. C. Pillai, P. Falaras, K. E. O'Shea, J. A. Byrne, D. D. Dionysiou, *J. Phys. Chem. Lett.* **2014**, *5*, 2543.
[69] S. Cong, J. Cai, X. Li, J. You, L. Wang, X. Wang, *Adv. Funct. Mater.* **2024**, *34*, 2401540.
[70] J. Xie, C. Zhang, T. D. Waite, *Water Res.* **2022**, *216*, 118319.
[71] S. Chai, G. Zhao, Y. Wang, Y.-n. Zhang, Y. Wang, Y. Jin, X. Huang, *Appl. Catal., B* **2014**, *147*, 275.
[72] J. Q. Chen, Z. J. Hu, N. X. Wang, *J. Environ. Sci. Health, Part B* **2012**, *47*, 579.
[73] S. Chen, Y. Liu, *Chemosphere* **2007**, *67*, 1010.
[74] M. Muneer, C. Boxall, *Int. J. Photoenergy* **2008**, *2008*, 197346.
[75] K. P. Gopinath, N. V. Madhav, A. Krishnan, R. Malolan, G. Rangarajan, *J. Environ. Manage.* **2020**, *270*, 110906.
[76] Y. Horiuchi, T. Toyao, M. Takeuchi, M. Matsuoka, M. Anpo, *Phys. Chem. Chem. Phys.* **2013**, *15*, 13243.
[77] H. S. Zakria, M. H. D. Othman, R. Kamaludin, S. H. Sheikh Abdul Kadir, T. A. Kurniawan, A. Jilani, *RSC Adv.* **2021**, *11*, 6985.
[78] S. G. Kumar, L. G. Devi, *J. Phys. Chem. A* **2011**, *115*, 13211.
[79] Q. Tian, W. Yao, W. Wu, C. Jiang, *Nanoscale Horiz.* **2019**, *4*, 10.
[80] H. Ji, W. Liu, F. Sun, T. Huang, L. Chen, Y. Liu, J. Qi, C. Xie, D. Zhao, *Chem. Eng. J.* **2021**, *419*, 129605.
[81] S. M. Fernandes, B. T. Barrocas, J. V. Nardeli, M. F. Montemor, E. Maçoas, M. C. Oliveira, C. C. C. R. de Carvalho, A. Lauria, M. Niederberger, A. C. Marques, *J. Environ. Chem. Eng.* **2024**, *12*, 112043.
[82] S. Amiri, M. Anbia, *J. Photochem. Photobiol., A* **2024**, *446*, 115146.
[83] S. Zhang, T. Hedtke, Q. Zhu, M. Sun, S. Weon, Y. Zhao, E. Stavitski, M. Elimelech, J.-H. Kim, *Environ. Sci. Technol.* **2021**, *55*, 9266.
[84] S. Nandy, S. A. Savant, S. Haussener, *Chem. Sci.* **2021**, *12*, 9866.
[85] S. Kundu, N. Karak, *Chem. Eng. J.* **2022**, *438*, 135575.
[86] N. Rosman, W. N. W. Salleh, M. A. Mohamed, J. Jaafar, A. F. Ismail, Z. Harun, *J. Colloid Interface Sci.* **2018**, *532*, 236.
[87] D. D. Phan, F. Babick, M. T. Nguyen, B. Wessely, M. Stintz, *Chem. Eng. Sci.* **2017**, *173*, 242.
[88] M. I. M. Ballari, R. Brandi, O. Alfano, A. Cassano, *Chem. Eng. J.* **2008**, *136*, 50.
[89] R. Lyubimenko, A. Turshatov, A. Welle, P. G. Weidler, B. S. Richards, A. I. Schäfer, *Chem. Eng. J.* **2023**, *451*, 138449.
[90] M. F. J. Dijkstra, A. Michorius, H. Buwalda, H. J. Panneman, J. G. M. Winkelman, A. A. C. M. Beenackers, *Catal. Today* **2001**, *66*, 487.
[91] S. Lotfi, K. Fischer, A. Schulze, A. I. Schäfer, *Nat. Nanotechnol.* **2022**, *17*, 417.
[92] S. Dekkouche, S. Morales-Torres, A. R. Ribeiro, J. L. Faria, C. Fontàs, O. Kebiche-Senhadji, A. M. T. Silva, *Chem. Eng. J.* **2022**, *427*, 131476.
[93] M. J. Arlos, M. M. Hatat-Fraile, R. Liang, L. M. Bragg, N. Y. Zhou, S. A. Andrews, M. R. Servos, *Water Res.* **2016**, *101*, 351.
[94] Q. Guo, C. Zhou, Z. Ma, X. Yang, *Adv. Mater.* **2019**, *31*, 1901997.
[95] R. A. Deshpande, J. Navne, M. V. Adelmark, E. Shkondin, A. Crovetto, O. Hansen, J. Bachmann, R. Taboryski, *Nat. Commun.* **2024**, *15*, 124.
[96] S. Riaz, S.-J. Park, *J. Ind. Eng. Chem.* **2020**, *84*, 23.
[97] G. R. Buettner, *Arch. Biochem. Biophys.* **1993**, *300*, 535.
[98] C. D. Vecitis, H. Park, J. Cheng, B. T. Mader, M. R. Hoffmann, *Front. Environ. Sci. Eng. China* **2009**, *3*, 129.
[99] J. M. Burns, W. J. Cooper, J. L. Ferry, D. W. King, B. P. DiMento, K. McNeill, C. J. Miller, W. L. Miller, B. M. Peake, S. A. Rusak, A. L. Rose, T. D. Waite, *Aquat. Sci.* **2012**, *74*, 683.
[100] S. Nonell, C. Flors, in, *Singlet Oxygen: Applications in Biosciences and Nanosciences* (Eds.: S. Nonell, C. Flors, S. Nonell, C. Flors), The Royal Society of Chemistry, London, UK, **2016**, pp. 2175-2181.
[101] A. V. Demyanenko, A. S. Bogomolov, N. V. Dozmorov, A. I. Svyatova, A. P. Pyryaeva, V. G. Goldort, S. A. Kochubei, A. V. Baklanov, *J. Phys. Chem. C* **2019**, *123*, 2175.
[102] M. Sun, H. Li, D. P. Jaisi, *Water Res.* **2019**, *163*, 114840.
[103] H. Li, A. F. Wallace, M. Sun, P. Reardon, D. P. Jaisi, *Environ. Sci. Technol.* **2018**, *52*, 1109.
[104] L. D. Freedman, G. O. Doak, *Chem. Rev.* **1957**, *57*, 479.
[105] W. Ma, J. He, L. Han, C. Ma, Y. Cai, X. Guo, Z. Yang, *Environ. Sci. Technol.* **2024**, *58*, 11625.
[106] Y. Guo, Y. Zhang, G. Yu, Y. Wang, *Appl. Catal., B* **2021**, *280*, 119418.
[107] J. M. Brownell, M. Chen, K. M. Parker, *Water Res.* **2025**, *274*, 123116.
[108] D. Minakata, W. Song, J. Crittenden, *Environ. Sci. Technol.* **2011**, *45*, 6057.
[109] D. Minakata, J. Crittenden, *Environ. Sci. Technol.* **2011**, *45*, 3479.
[110] M. Sadatsharifi, D. W. Ingersoll, M. Purgel, *Environ. Sci.: Processes Impacts* **2021**, *23*, 1018.
[111] D. P. Jaisi, H. Li, A. F. Wallace, P. Paudel, M. Sun, A. Balakrishna, R. N. Lerch, *J. Agric. Food Chem.* **2016**, *64*, 8474.
[112] A. G. Albesa, M. E. F. Hermosilla, *Chem. Phys. Impact* **2023**, *6*, 100140.
[113] A. Karton, in, *Annual Reports in Computational Chemistry* (Ed.: D.A. Dixon), Elsevier, Amsterdam, Netherlands, **2022**, pp. 123-166.
[114] B. Fiser, B. Jójárt, M. Szőri, G. Lendvay, I. G. Csizmadia, B. Viskolcz, *J. Phys. Chem. B* **2015**, *119*, 3940.
[115] Z. B. Rózsa, A. Rágyanszki, B. Viskolcz, M. Szőri, *Comput. Theor. Chem.* **2023**, *1225*, 114162.
[116] L. A. Curtiss, K. Raghavachari, P. C. Redfern, V. Rassolov, J. A. Pople, *J. Chem. Phys.* **1998**, *109*, 7764.
[117] A. G. Baboul, L. A. Curtiss, P. C. Redfern, K. Raghavachari, *J. Chem. Phys.* **1999**, *110*, 7650.
[118] D. Papagiannaki, C. Medana, R. Binetti, P. Calza, P. Roslev, *Sci. Rep.* **2020**, *10*, 20247.
[119] A. Serra-Clusellas, L. De Angelis, M. Beltramo, M. Bava, J. De Frankenberg, J. Vigliarolo, N. Di Giovanni, J. D. Stripeikis, J. A.

Rengifo-Herrera, M. M. Fidalgo de Cortalezzi, *Environ. Sci.:Water Res. Technol.* **2019**, *5*, 1932.
[120] A. Grandcoin, S. Piel, E. Baurès, *Water Res.* **2017**, *117*, 187.
[121] C. P. M. Bento, X. Yang, G. Gort, S. Xue, R. van Dam, P. Zomer, H. G. J. Mol, C. J. Ritsema, V. Geissen, *Sci. Total Environ.* **2016**, *572*, 301.
[122] Y. Huang, Z. Li, K. Yao, C. Chen, C. Deng, Y. Fang, R. Li, H. Tian, *Appl. Catal., B* **2021**, *299*, 120671.
[123] S. M. Ilina, P. Ollivier, D. Slomberg, N. Baran, A. Pariat, N. Devau, N. Sani-Kast, M. Scheringer, J. Labille, *Environ. Sci.: Nano* **2017**, *4*, 2055.
[124] R. Chang, in *Chemistry*, 10th ed., McGraw-Hill Education, Columbus, Ohio, USA, **2009**.
[125] M. Ndjeri, A. Pensel, S. Peulon, V. Haldys, B. Desmazières, A. Chaussé, *Colloids Surf. A* **2013**, *435*, 154.
[126] S. Venditti, A. Kiesch, J. Hansen, *Chemosphere* **2023**, *340*, 139843.
[127] S. Liu, E. Véron, S. Lotfi, K. Fischer, A. Schulze, A. I. Schäfer, *J. Hazard. Mater.* **2023**, *447*, 130832.
[128] J. M. Herrmann, *Top. Catal.* **2005**, *34*, 49.
[129] E. Worch, *Vom Wasser* **1993**, *81*, 289.
[130] Z. Wang, J. Liu, Y. Dai, W. Dong, S. Zhang, J. Chen, *Ind. Eng. Chem. Res.* **2011**, *50*, 7977.
[131] B. Byrne, J. Liu, K. W. Bowman, M. Pascolini-Campbell, A. Chatterjee, S. Pandey, K. Miyazaki, G. R. van der Werf, D. Wunch, P. O. Wennberg, C. M. Roehl, S. Sinha, *Nature* **2024**, *633*, 835.
[132] W. Yan, C. Jing, *Environ. Sci. Technol.* **2018**, *52*, 1946.
[133] S. Doyle, M. Garvey, C. Fowley, *Environ. Nanotechnol., Monit. Manage.* **2023**, *20*, 100839.
[134] Y. Yao, H. Chen, C. Lian, F. Wei, D. Zhang, G. Wu, B. Chen, S. Wang, C. Fe, *J. Hazard. Mater.* **2016**, *314*, 129.
[135] S. G. Patra, A. Mizrahi, D. Meyerstein, *Acc. Chem. Res.* **2020**, *53*, 2189.
[136] Y. Guo, J. Long, J. Huang, G. Yu, Y. Wang, *Water Res.* **2022**, *215*, 118275.
[137] W. Zhang, Q. You, J. Shu, A. Wang, H. Lin, X. Yan, *Front. Environ. Sci.* **2023**, *11*, 2023 .
[138] O. Holtomo, M. D. Mbigah, M. Nsangou, O. Motapon, *RSC Adv.* **2021**, *11*, 16404.
[139] M. Narimani, G. da Silva, *Environ. Sci.: Processes Impacts* **2020**, *22*, 152.
[140] A. Imbrogno, A. I. Schäfer, *J. Membr. Sci.* **2019**, *585*, 67.
[141] K. Fischer, P. Schulz, I. Atanasov, A. Abdul Latif, I. Thomas, M. Kühnert, A. Prager, J. Griebel, A. Schulze, *Catalysts* **2018**, *8*, 376.
[142] A. Schulze, M. F. Maitz, R. Zimmermann, B. Marquardt, M. Fischer, C. Werner, M. Went, I. Thomas, *RSC Adv.* **2013**, *3*, 22518.
[143] Health Canada, in *Guidelines for Canadian drinking water quality operational parameters*, **2024**, https://www.canada.ca/en/health-canada/programs/guidelines-canadian-drinking-water-quality-operational-parameters.html.
[144] P. B. Trinh, A. I. Schäfer, *J. Hazard. Mater.* **2023**, *454*, 131211.
[145] L. Wang, X. Lan, W. Peng, Z. Wang, *J. Hazard. Mater.* **2021**, *408*, 124436.
[146] R. Dennington, T. A. Keith, J. M. Millam, in *Semichem Inc*, Shawnee Mission, Kansas, **2016**.
[147] A. V. Marenich, C. J. Cramer, D. G. Truhlar, *J. Phys. Chem. B* **2009**, *113*, 6378.
[148] R. Janoschek, M. J. Rossi, *Int. J. Chem. Kinet.* **2002**, *34*, 550.
[149] M. J. Frisch, G. W. Trucks, H. B. S. Schlegel, M. A. Robb, J. R. Cheeseman, G. Scalmani, V. Barone, G. A. Petersson, H. Nakatsuji, X. Li, M. Caricato, A. V. Marenich, J. Bloino, B. G. Janesko, R. Gomperts, B. Mennucci, H. P. Hratchian, J. V. Ortiz, A. F. Izmaylov, J. L. Sonnenberg, Y, D. Williams, F. Ding, F. Lipparini, F. Egidi, J. Goings, B. Peng, A. Petrone, T. Henderson, Gaussian, Gaussian, Inc, Wallingford CT, **2016**.
[150] A. Imbrogno, M. N. Nguyen, A. I. Schäfer, *Chemosphere* **2024**, *357*, 141833.